SURFACE HARDENING OF STEELS BY USING A CO_2 LASER WITH BLACK COLOR COATING

MR. BHAVIN BHATRASUPONG

AN INDEPENDENT STUDY SUBMITTED IN PARTIAL FULFILLMENT
OF THE REQUIREMENTS FOR
THE DEGREE OF MASTER OF ENGINEERING (METALLURGICAL ENGINEERING)
FACULTY OF ENGINEERING
KING MONGKUT'S UNIVERSITY OF TECHNOLOGY THONBURI
2013

Surface Hardening of Steels by using a CO_2 Laser with Black Color Coating

Mr. Bhavin Bhatrasupong B.Ind.Tech.(Electronic)

An Independent Study Submited in Partial Fulfillment
of the Requirements for
the Degree of Master of Engineering (Metallurgical Engineering)
Faculty of Engineering
King Mongkut's University of Technology Thonburi
2013

Independent Study Committee

.....Chairman of Independent Study Committee
(Assoc. Prof. Chaowalit Limmaneevichitr, Ph.D.)

.....Independent Study Advisor
(Paiboon Choungthong, Dr.Ing.)

.....Independent Study Advisor
(Viboon Tangwarodomnukun, Ph.D.)

.....Committee
(Supparerk Boontein, Ph.D.)

หัวข้อการค้นคว้าอิสระ	การเพิ่มความแข็งผิวโลหะด้วยคาร์บอนไดออกไซด์เลเซอร์และการเคลือบผิวด้วยสีดำ
หน่วยกิต	6
ผู้เขียน	นายภวินญ์ ภัทรสุพงศ์
อาจารย์ที่ปรึกษา	ดร.ไพบูลย์ ช่วงทอง ดร.วิบุญ ตั้งวโรดมนุกูล
หลักสูตร	วิศวกรรมศาสตรมหาบัณฑิต
สาขาวิชา	วิศวกรรมโลหการ
ภาควิชา	วิศวกรรมอุตสาหการ
คณะ	วิศวกรรมศาสตร์
ปีการศึกษา	2556

บทคัดย่อ

การเพิ่มความแข็งที่ผิวโลหะกลุ่มเหล็กกล้าด้วยแสงเลเซอร์ ซึ่งพลังงานความร้อนของแสงเลเซอร์จะเปลี่ยนเฟสจากออสเตนไนท์ ไปเป็นมาร์เทนไซด์ โดยการควบคุมลำแสงเลเซอร์ยิงไปยังผิวของเหล็กกล้าที่มีส่วนผสมคาร์บอนมากกว่า 0.1 % ซึ่งเป็นอุณหภูมิในช่วงที่สามารถเกิดเป็นเฟสออสเตนไนท์ได้ จากนั้นอุณหภูมิจะเย็นตัวอย่างรวดเร็วจนคาร์บอนแพร่ออกไม่ทัน ทำให้กลายเป็นเฟสมาร์เทนไซด์ ซึ่งมีความแข็งมาก ขั้นตอนในการชุบแข็งด้วยเลเซอร์โดยทั่วไป จะใช้เลเซอร์กำลังสูงที่มากกว่า 400 W และระบบควบคุมที่ทันสมัยเพื่อควบคุมการเกิดอุณหภูมิที่ผิวได้ ประกอบกับการใช้วัสดุที่มีประสิทธิภาพในการดูดกลืนสูง เคลือบที่ผิวเพื่อลดการสะท้อนที่ผิวอย่างเช่นกราไฟต์ การวิจัยเชิงทดลองนี้ จะจัดทำชุดทดลองต้นแบบ ซึ่งประยุกต์ใช้คาร์บอนไดออกไซด์เลเซอร์กำลังต่ำขนาด 40 W และชุดควบคุมความเข้ม และการเคลื่อนที่ของแสงเลเซอร์ และใช้การเคลือบด้วยสีดำ เพื่อลดการสะท้อนที่ผิว ทดลองกับเหล็กเกล้า 2 เกรด คือ AISI 4140 และ AISI 1045 โดยผลการทดลอง สามารถเพิ่มความแข็งที่ผิวของเหล็กได้ทั้งสองเกรด ได้ค่าความแข็งประมาณ 700 ถึง 800 HV และชั้นความแข็งลึกประมาณ 90 ไมครอน

คำสำคัญ : คาร์บอนไดออกไซด์เลเซอร์ / การชุบแข็งด้วยเลเซอร์ / เหล็กกล้า

Independent Study Title	Surface hardening of steels by using a CO_2 laser with black color coating
Credits	6
Candidate	Mr.Bhavin Bhatrasupong
Independent Study Advisors	Dr.Paiboon Choungthong
	Dr.Viboon Tangwarodomnukun
Program	Master of Engineering
Field of Study	Metallurgical Engineering
Department	Production Engineering
Faculty	Engineering
Academic Year	2013

Abstract

Surface hardening of steels with a laser beam uses the concept of the phase transformation from austenite to martensite. This is achieved by controlling movement and focus of the laser beam over the surface of steel containing more than 0.1 % carbon to acquire a desired temperature. As the laser beam moves away, the temperature drops rapidly to prevent carbon diffusion. This produces a hard martensite structure. A typical laser hardening procedure requires a high power laser, generally in excess of 400 W to maintain an adequate power density, incorporating with a complex and expensive control system. To minimize surface reflection, the steel being treated is often coated with an expensive and high efficiency absorber such as graphite. The purpose of this experiment is to introduce a lower cost alternative. A trial consisting of a 40 W carbon dioxide laser, a modestly priced control system, and a common flat black color coating to reduce surface reflection was tested on the two grades of steel samples are: AISI 4140, and AISI 1045. The results showed that the hardness of the steel surface in both grades can be remarkably increased, where the hardness of about 700 to 800 HV with the depth of about 90 microns can be achieved.

Keywords : CO_2 Laser / Laser Surface Hardening / Steels

ACKNOWLEDGEMENTS

I would like to thank those individuals whose help made this independent study possible:

- Dr.Paiboon Choungthong and Dr.Viboon Tangwarodomnukun, King Mongkut's University of Technology Thonburi, who helps and advises me.

- Miss Bheemaya Bhatrasupong, who supports scholarship and encouragement.

- Mr.Manthep Khajonkultham and Engineering Service Center, College of Engineering, Rangsit University, supported workshop, tooling, materials and other.

- Mr.Payoon Senthongkaew and Department of Materials Engineering, Faculty of Engineering, Kasetsart University, supported SEM.

- Mr.Brent Schumacher, Civil Engineer, United States Department of Agriculture, who checked English grammar.

CONTENTS

LIST OF TABLES

LIST OF FIGURES

LIST OF SYMBOLS AND ABBREVIATIONS

%	=	percentage
µm	=	micrometer
ºC	=	degree Celsius
ºF	=	degree Fahrenheit
wt%	=	percent by weight
α	=	Thermal diffusivity (m^2/s)
AISI	=	American Iron and Steel Institute
Al	=	aluminum
ArF	=	argon-fluoride
ASTM	=	American Society for Testing and Materials
BCC	=	Body-Centered Cubic
BCT	=	Body-Centered Tetragonal
C	=	carbon
CCT	=	Continuous Cooling Transformation
cm	=	centimeter
CNC	=	Computer Numerical Control
Co	=	cobalt
CO_2	=	carbon dioxide
Cr	=	chromium
Cu	=	copper
CW	=	Continuous Wave
DOF	=	Depth of field, Depth of focus
Er:YAG	=	Erbium-doped Yttrium Aluminum Garnet
RZ	=	Removal zone
FCC	=	Face-Centered Cubic
Fe	=	ferrous
FZ	=	Fusion Zone
g	=	gram
Ge	=	germanium
HAZ	=	Heat Affected Zone
HeCd	=	helium-cadmium
HeNe	=	helium-heon
HV	=	Vickers hardness
ISO	=	International Organization for Standardization
J	=	joule
JIS	=	Japanese Industrial Standards
k	=	Thermal conductivity (W/(m·K))
KrF	=	krypton-fluoride
kV	=	kilo-voltage
kW	=	kilo-watt
Laser	=	Light Amplification by Stimulated Emission of Radiation
mA	=	milliampere
M_f	=	Martensite finish temperature
Mg	=	magnesium
mm	=	millimeter
Mn	=	manganese
Mo	=	molybdenum

MoS_2	=	molybdenum disulfide
MPa	=	megapascal
M_s	=	Martensite start temperature
N_2	=	nitrogen
NA	=	Not Available
Nd:YAG	=	Neodymium-doped Yttrium Aluminum Garnet
Nd:YLF	=	Neodymium-doped Yttrium Lithium Fluoride
Ni	=	nickel
Nital	=	Nitric acid solution in alcohol
OEM	=	Original Equipment Manufacturer
OM	=	Optical Microscope
P	=	phosphorous
RPM	=	Rounds Per Minute
S	=	sulfur
s	=	second
SEM	=	Scanning Electron Microscope
Si	=	silicon
TEM_{xx}	=	Transverse Electromagnetic Mode
Ti	=	titanium
V	=	vanadium
Vdc	=	Voltage direct current
W	=	watts
ZnSe	=	zinc-selenide

CHAPTER 1 INTRODUCTION

1.1 Problem statements

Laser hardening is a heat treatment process for improving the wear resistance or surface hardening by using a laser beam to heat the surface of steel to a period of hardening temperature, just under the melting temperature. This treatment is used on steel or cast iron with carbon content more than 0.1 %. As the laser moves away, the hot layer will be cooled very rapidly by the steel surrounding the area by a process known as "self-quenching", which is a phenomenon of the laser hardening process. Rapid cooling will prevent the steel lattice from returning to its original structure. The microstructure will change from Austenite to Matensite, increasing the hardness of the steel.

The purpose of this experimental research is to study, investigate, and gauge the effectiveness of a low cost laser hardening method. Other research has used high power lasers, exceeding 400 W, with advanced technology control systems, and high efficiency graphite coatings for the work pieces to minimize surface reflection [1, 2]. For this experiment, a trial will be prepared consisting of a 40 W carbon dioxide laser, a low cost readily available control system, and common flat black color coating for the steel samples to reduce surface reflection.

Theory and parameters that affect surface temperatures, structure of resulting martensites, durability and surface removal resistance were investigated in detail. The hardness and thickness of affected layers of the sample steels were measured with an optical microscope (OM), micro-hardness tester and analyzed with a scanning electron microscope (SEM) to conclude this research.

1.2 Objectives of the study

To increase the hardness of a steel surface with a 40 W CO_2 laser.

1.3 Outline of the study

1. Prepare the experiment consisting of a carbon dioxide laser, and apparatus needed to control the intensity and movement of the laser beam.
2. Study the theory and parameters that affect surface temperature, the martensites structure, hardness and thickness of the layers.
3. Testing and analyzing the results of treated samples with an OM micro-hardness tester and SEM.

1.4 Benefits of the study

The study and results of this experiment, using a CO_2 laser specifically for laser surface hardening, will have additional applications relating to surface heat treatment, laser coating, laser cutting, laser welding, and other functions; upon further examination of the power requirements for the CO_2 laser.

CHAPTER 2 THEORIES AND LITERATURE REVIEWS

This chapter will separated into four parts: concept of a CO_2 laser surface hardening, transformation hardening of each phase transformation, influential factors affect to hardness and literature review.

2.1 Laser surface hardening

Since 1916, Albert Einstein had proposed the theory of stimulated emission of radiation, stating that photons could stimulate emission of identical photons from excited atoms. The first ruby laser was demonstrated at Hughes Research Labs in 1960. Kumar Patel made a CO_2 laser at Bell Labs in 1964. A brief timeline of laser technology development history [3] is shown in Appendix A. With current technology, laser beam emission ranges almost all wavelengths from infrared, visible light, ultraviolet to X-rays; as shown in Appendix B: Electromagnetic Spectrum [4]. There is a variety of laser processes; both continuous wave mode and pulse wave mode; classified by category of active medium: Solid state, gas, and liquid; shown in Appendix C: Types of Industrial Lasers [4].

The concept of laser hardening is in principle similar to the normal hardening processes. Heat energy generated by the laser beam focuses to surface of material, quickly heating up the irradiated area to above the critical temperature of solid-state transformation, but below the melting temperature. The heated material undergoes a transformation change from ferrite to austenite. As the laser moves away, the surrounding material cools the surface rapidly by thermal conduction. Because the heat is generated in a very small area the material will have a self-quenching effect. This allows for the transformation from austenite to martensite as shown in Figure 2.1. When the power of the laser is increased to achieve a temperature above the melting point, the steel is expected to melt at the surface. If the power of the laser is increased to generate a temperature above the boiling point; surface vaporization will occur resulting in a loss of base steel at the surface.

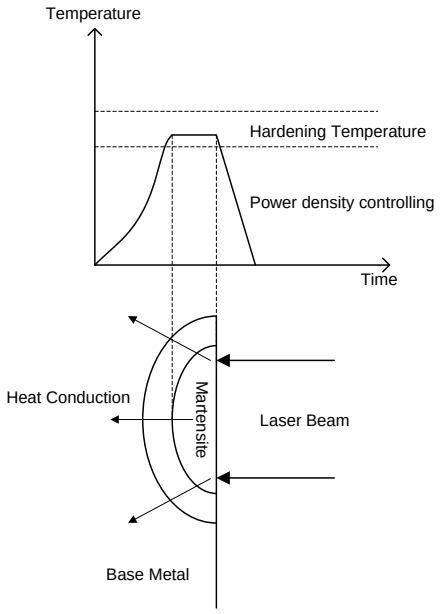

Figure 2.1 Principle of laser surface hardening

Therefore, laser surface hardening is widely used to harden localized areas and small size parts that required partial of steel and cast iron machine components or other such as gear.

2.2 Transformation hardening

As Figure of appendix D presents iron-carbon equilbrium diagram, two steps of structure changing are formation of austenite and martensite. The production of martensite structure depends on temperature transformation of the crystal structure of iron and redistribution of carbon content within the thermal cycle as follow as Figure 2.2 (a).

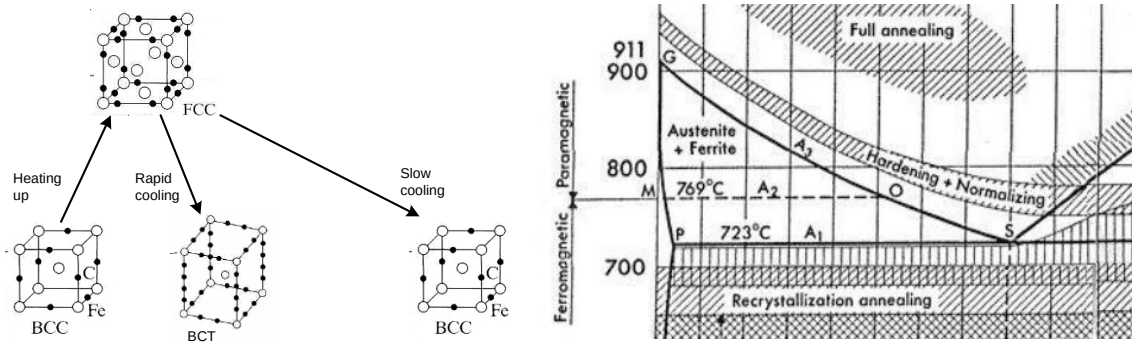

(a) Martensite transformation diagram (b) A1 and A3 line

Figure 2.2 Equilibrium transformation

2.2.1 Austenite transformation

Austenite is formed from pearlite-ferrite or pearlite-cementite or martensite in case of passed hardening heat treatment. In the heating phase, the Body-Centered Cubic (BCC) transforms to Face-Centered Cubic (FCC). In equilibrium transformation, austenite starts to form at A1 line as Figure 2.2 (b) and completes at A3 line. Since the heating rate is quite high, the A3 line tends to move upwards to a higher temperature because the equilibrium condition. Therefore, in order to achieve sufficient homogenization of austenite above the A3 temperature, the process parameters are normally set to produce high peak temperatures. The short thermal cycle of laser beam may cause insufficient carbon diffusion; the degree of homogenization of carbon in the base material has a significant influence on the carbon distribution of formed martensite and the produced hardness value [5].

2.2.2 Martensite transformation

Martensite is formed from γ-solid to α-solid, in which γ-lattice change to the α-lattice. Full or 100% martensitic transformation initiate with relatively high cooling rate. In this case, carbon atoms solved in the γ-austenite do not have enough time to precipitate and remain in the transforming lattice. Therefore, martensite is a supersaturated solution of carbon in α-iron. The trapped carbon atoms in the lattice result in few shift of the iron atoms and thus a Body-Centered Tetragonal (BCT) lattice is formed as shown in Figure 2.2 (a). In the cooling phase, transformation of austenite to martensite starts from the martensite start (M_s) temperature and ends at the martensite finish (M_f) temperature. Martensite is formed over a few temperature ranges, which depending on the carbon content of steel, as shown in Figure 2.3. As the temperature achieves the M_s temperature in the cooling phase, the cooling rate is required to exceed the critical cooling rate at the M_f temperature in order to produce 100% martensite [5].

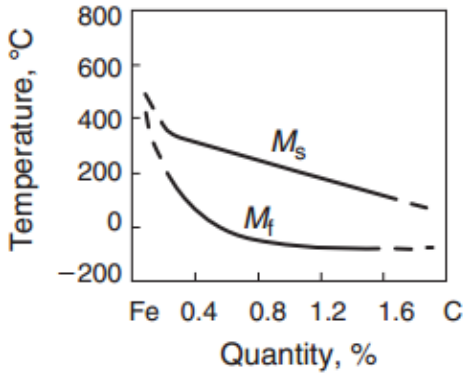

Figure 2.3 M_s and M_f versus carbon content [5]

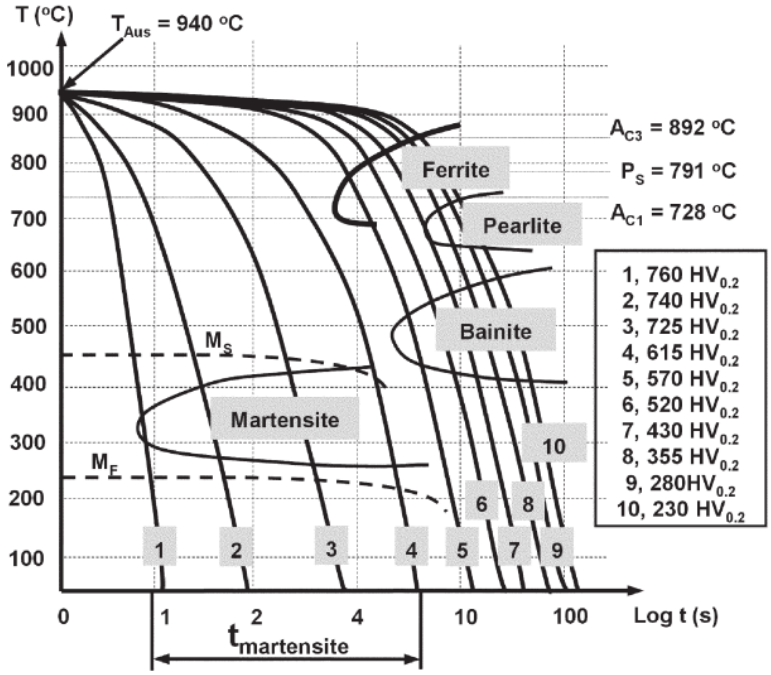

Figure 2.4 Continuous Cooling Transformation (CCT) diagram [6]

Figure 2.4 present the continuous cooling transformation (CCT) diagram for eutectoid carbon steel. The line number one to number four is the region with higher cooling rate which produces 100% martensite as well. The line number five to number seven is the bainite transformation and the line number eight to number ten is pearlite transformation. In laser hardening, the cooling rate by heat conduction into the substrate is normally high enough for 100% martensitic transformation even in low carbon steel [6].

2.2.3 Retained austenite

Retained austenite occurs when steel is not quenched to the M_f temperature or martensite finish temperature. There are multiple factors that may cause this, such as too slow of a cooling rate, quenching from too high of a case austenite temperature, local carbon concentration due to the inhomogeneity of material and existence of the austenite stabilizing elements.

2.3 Influential factors

There are many factors can be influenced to the laser hardening process as follows [1, 7].

2.3.1 Material properties

Chemical composition: Carbon content affects the formation of martensite and surface hardness. The material for laser hardening should typically contain at least 0.05 wt% carbon. The surface hardness generally increases linearly with 0.05 wt% to 0.6 wt% carbon ranges and higher than about 0.6 wt% may result in a much higher amount of retained austenite present at room temperature which reduce the surface hardness. Other elements such as Mn, Cr, Ni and Mo will increases the volume of retained austenite and influence to thermal properties.

Thermal properties consist of thermal conductivity and thermal diffusivity. Thermal conductivity or heat conduction is the property of a material's ability to conduct heat. It is measured in W/(K.m) or in IP units (Btu/(hr.ft.F)). Thermal diffusivity is thermal conductivity divided by density and specific heat capacity. Thermal diffusivity relates a materials ability to conduct thermal energy relative to the materials ability to store thermal energy; measured in m^2/s.

Surface roughness affects the materials ability to reflect or absorb radiation. A rough surface will absorb more laser irradiation than a flat smooth surface. Increasing the surface roughness of steel to a scale much larger than the laser wavelength may increase the absorptivity of laser energy, depending on the material and the type of laser.

2.3.2 Laser parameters

Power of the laser: The energy of output of laser tube is measured in watts regardless laser beam diameter. The lens can determine the specific beam diameter of a laser. Therefore, the power of laser in relation to the beam diameter is also known as power density, measured in W/cm^2. Power density, in combination with interaction time or energy density will affect surface temperature. Laser hardening requires a power density of 10^3-10^5 W/cm^2 or heating area as shown in Figure 2.5.

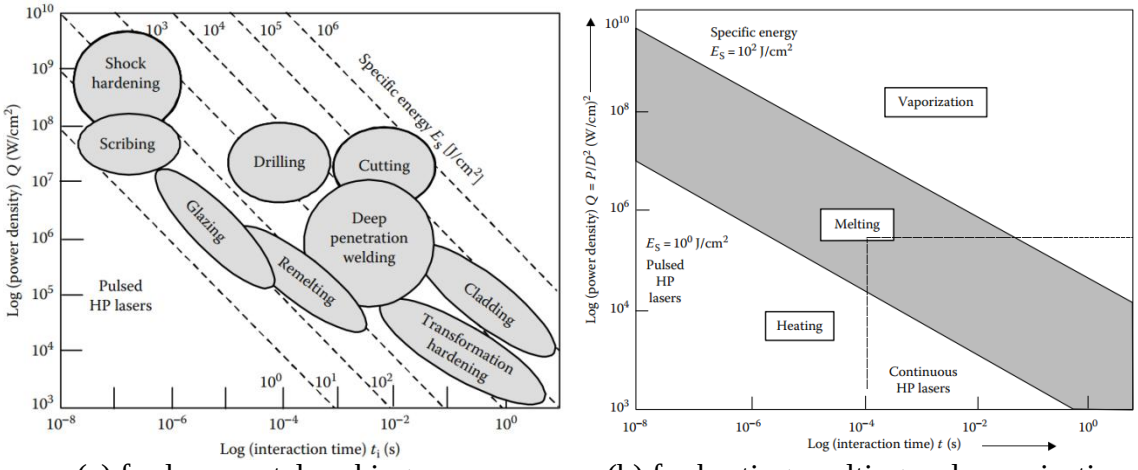

(a) for laser metalworking processes (b) for heating, melting and vaporization

Figure 2.5 Energy density [1]

Beam diameter at focus (d_f = 0.237 mm) can be calculated from equation 2.1 [1] and other variables from laser system specifications as appendix E. The lambda (λ = 10.6 μm) is the wavelength of CO_2 laser. The focal length (F = 50.8 mm) is the distance from the center of the lens to the focal point. The M = 1.1 is the laser beam quality and the d_B = 3.5 mm is beam diameter at output of CO_2 laser tube or before into the focus lens.

$$d_f = \frac{4\lambda F M^2}{\pi d_B} \tag{2.1}$$

Depth of field (Z_f = 5.686 mm) is also known as the depth of focus is a measure of the change in the waist of the beam on either side of the focal plane as present in Figure 2.6 and can be calculated from equation 2.2 [1]. It is often defined as the distance along the axis over which the focused spot size increases by 5%, or the distance over which the intensity exceeds half the intensity at focus.

$$Z_f = \frac{8\lambda}{\pi}\left(\frac{F}{d_B}\right)^2 = \frac{8\lambda f^2}{\pi} = 2fd_f. \tag{2.2}$$

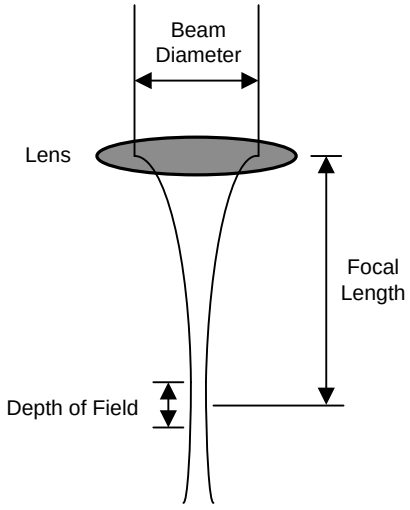

Figure 2.6 Depth of field

Beam profile, the transverse electromagnetic mode is very important in the interaction with the workpiece material because mean that level of energy of laser beam to area of surface of material steady or not, controlling temperature at surface by controlling power density of laser beam is to be concerned. Theoretical of CO_2 laser is TEM_{00} or called "Gaussian beam" as shows in Figure 2.7 (a), and TEM_{00} is ideal for cutting and drilling when focused with a convergent lens to a very small area thus providing a very high power density, and can used. For multimode beam structures TEM_{01}, TEM_{10}, TEM_{11}, and TEM_{20} is higher-order mode of transverse power density distribution in terms of radius (ρ) and angle (ϕ) or form $TEM_{\rho\phi}$. Projection of laser beam will related with peak amplitude of wavelength, thus higher peak amplitude will higher power density.

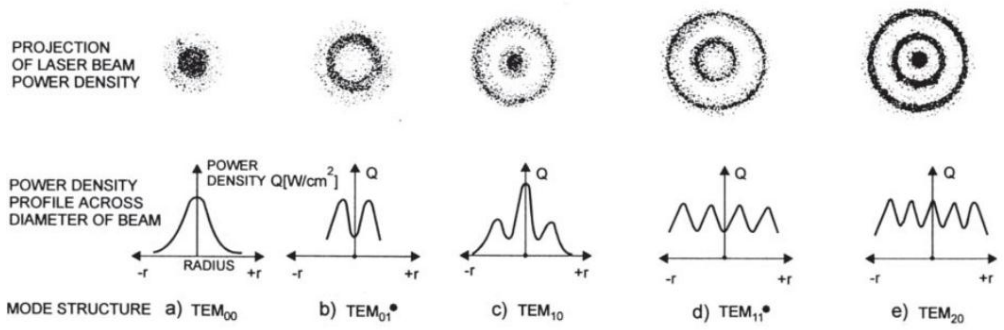

Figure 2.7 Basic laser beam mode structures [7]

2.3.3 Absorption of laser radiation

As Figure 2.8 shows when laser beam incident to material will result in four types of radiation distribution: Reflection, absorption, transmission and scattering. Refection and absorption is mainly influenced by the wavelength of laser, surface coating, angle of incident and temperature at the surface.

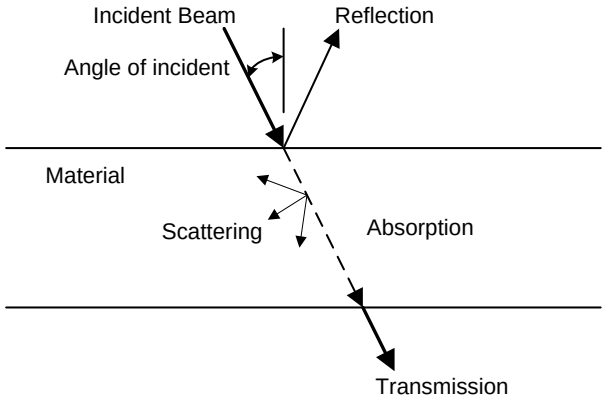

Figure 2.8 Incident beam to material

Wavelength of laser will affect the absorption of laser radiation towards each material with ferrous and nonferrous. Figure 2.9 shows the reflectivity of CO_2 laser radiation by steel to be about 90%; low when compared with other types of lasers.

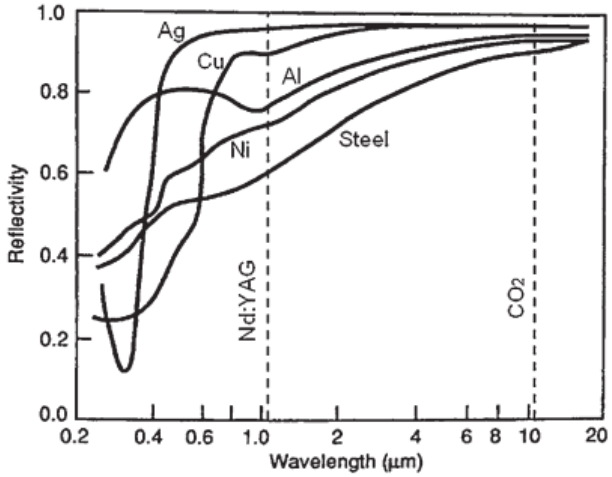

Figure 2.9 Variation of reflectivity with wavelength for several metallic materials [4]

Surface coating with absorbers, oxide film, surface roughness, or other condition affect to absorption and reflection. Figure 2.10 shows influences exerted on absorptivity of CO_2 and Nd:YAG laser light in interaction with specimens made of Ck 45 steel in various condition such as polished, grounded, turned, sandblasted, oxidized and graphitized, which obviously seen that absorption be significant at most caused absorption be obstacle to temperature controlling at surface of material.

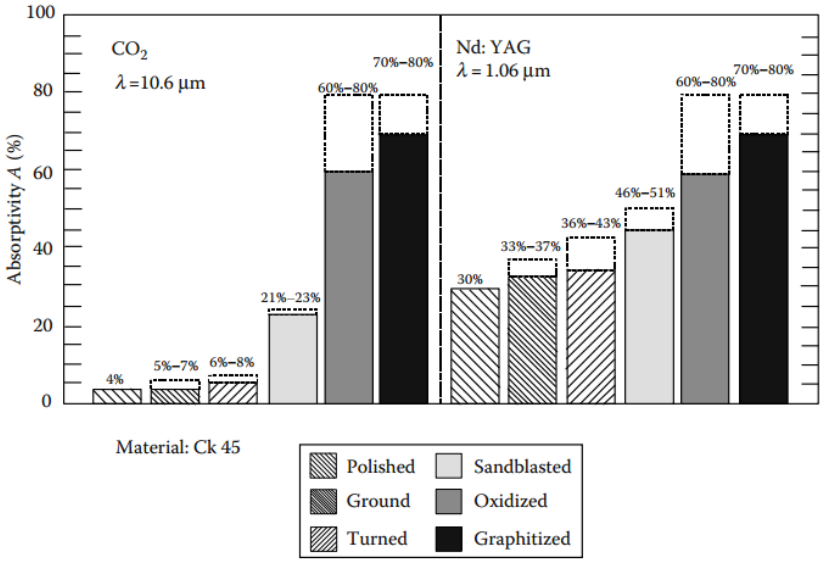

Figure 2.10 Influence of various steel Ck 45 treatments on absorption [1]

Angle of incident affects absorption ability, because of the polarization plane of the laser. A zero degree angle of incidence will have percent reflection about 80-90% as shown in Figure 2.11.

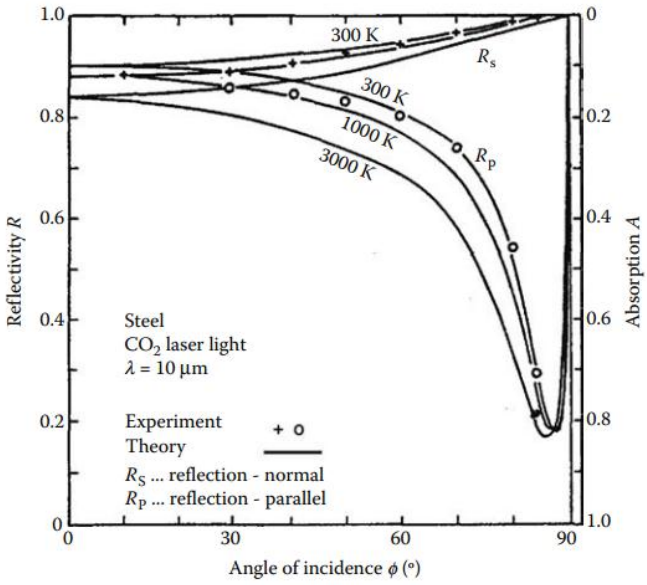

Figure 2.11 Variation of reflectivity with angle and plane of polarization [1]

Temperature at the surface causes a change in status of the surface from solid, to liquid and gas. However, each status affects reflection ability. At the melting temperature 60% to 95% of the laser light is reflected. Below the melting temperature for a coated surface

just 5% to 10% of the light is reflected. The problem of reflection as it relates to temperature is more pronounced for laser heat treatment work, than it is for laser cutting work.

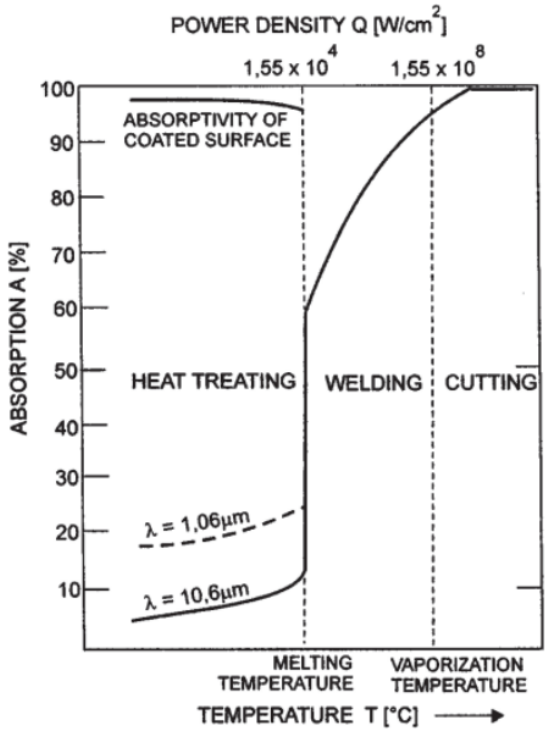

Figure 2.12 Effect of temperature on laser light absorptivity [7]

2.3.4 Process parameters

The travelling speed is a normal the parameter that is set to optimize the process in order to obtain the required hardened depth. The slower the traveling speed the more time is allowed for thermal conductivity resulting in an increase in the hardened depth. Figure 2.12 shows laser power and travelling speed versus depth of hardened layer for 4140 steel.

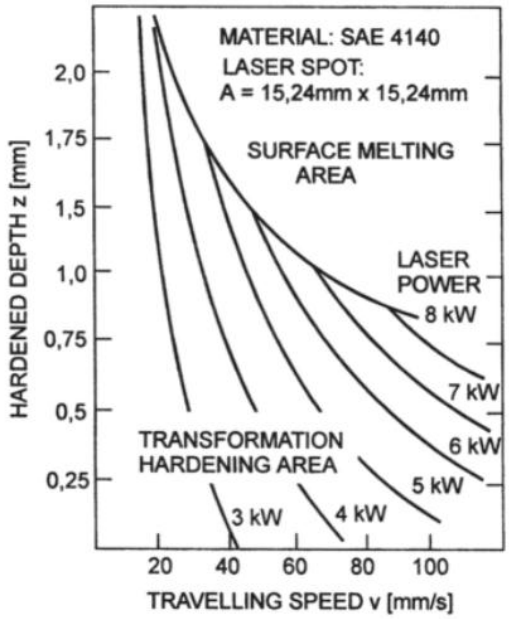

Figure 2.13 Travelling speed versus depth of hardened layer [7]

2.4 CO_2 laser

The CO_2 laser has proven to be very versatile for use in industry due to its relatively low cost, simple construction, and ease of operation and maintenance. Additionally, the CO_2 laser is compatible with a broad domain of power application, ranging from 30 W to 8,000 W. At present there are many types of industrial lasers as seen in Appendix C. The CO_2 laser was chosen for this research because of its ease of set up, functional tooling ability, relatively simple operation and maintenance characteristics, and its low cost. However, the major drawback would be the 10.6 μm beam wavelength of the CO_2 laser makes it more difficult for absorption in steels than a more specialized laser with a shorter wavelength. While less than optimum, the ease of tooling was the primary consideration, making the CO_2 laser the first choice.

2.4.1 Basic physics of excitation

The CO_2 laser operates by use of energy exchanges between pairs of molecule in form of triatomic molecule and vibration of its. As Figure 2.14 shows three vibration mode with one non-vibration mode is unexcited mode (a). The symmetric stretch mode (ν_1), the oxygen atoms vibrate in a straight line in opposition to each other. The bending mode (ν_2), the oxygen atoms can oscillate in two planes perpendicular to the principal molecular axis. The asymmetric stretch mode (ν_3), the oxygen atoms are always moving in the same direction along the axis.

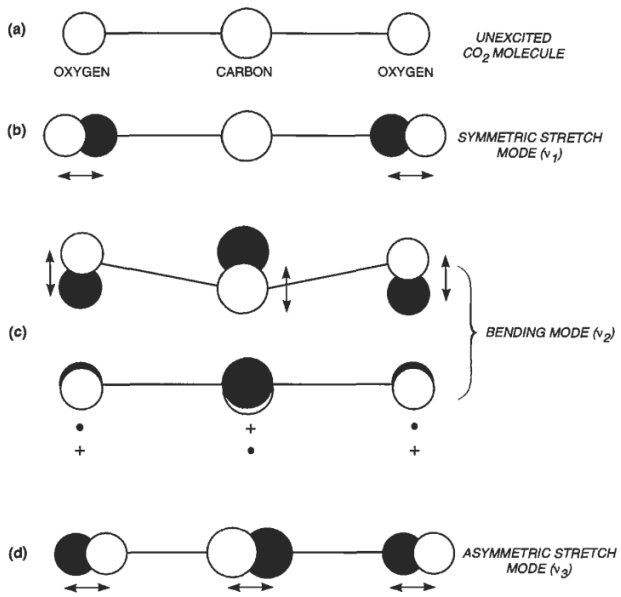

Figure 2.14 CO_2 molecular structure and three fundamental modes of vibration [8]

Vibrational level of CO_2 molecule are characterized in terms of the quantum numbers, n_1,n_2,n_3, which refer to the number of quanta of energy in each of the vibrational modes with two energy levels for ν_1 and ν_3 and three energy levels for ν_2. In case of vibrational level of N_2 molecule, there is only one quantum numbers (ν) with two energy levels as shown in Figure 2.15.

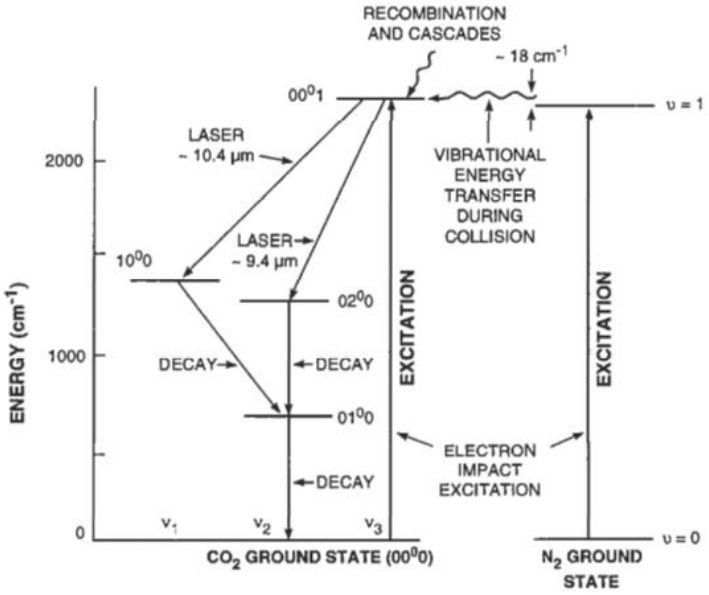

Figure 2.15 Energy level diagram of CO_2 and N_2 molecular [8]

2.5 Literature reviews

J. Senthil Selvan et al (1999) [9] studied effects of laser surface hardening on AISI 5135 steel for improve the tribological properties and also to increase the service life of automobile components such as camshafts, crankshafts, lorry brake drums and gears by applied 1300 W and 1500 W CO_2 lasers with MoS_2 coating. Results are the laser-hardened process increases the hardness of the base steel from 250 to 900 $HV_{0.2}$ as Figure 2.16. A three-fold increase in hardness was obtained with a maximum case depth of 0.45 and 0.65 mm laser powers of 1.3 and 1.5 kW respectively, absorption coefficient of MoS_2 coating is 70 %. The microstructures consist of white martensite plates 1–2 mm in size with undissolved carbides in the middle of the laser-treated zone, radial martensites of a larger size at the surface and large carbides in HAZ.

Laser power, q (w)	1300	1500
Beam diameter, d (mm)	3.0	3.0
Scan speed, v (m min^{-1})	1.0	1.0
Interaction time, t (s)	0.18	0.18
Surface coating	MoS_2	MoS_2
Coupling coefficient, A[a]	0.70	0.70
Power density (W cm^{-2})[a]	1.3×10^{-4}	1.5×10^{-4}
Energy density (kJ cm^{-2})[a]	2.3	2.7
Cooling rate (°C s^{-1})[a]	4283	5030
Surface temperature T (°C)[a]	1207	1400
Predicted case depth (mm)[a]	0.65	0.75
Measured case depth (mm)[a]	0.45	0.65

(a) Process parameter

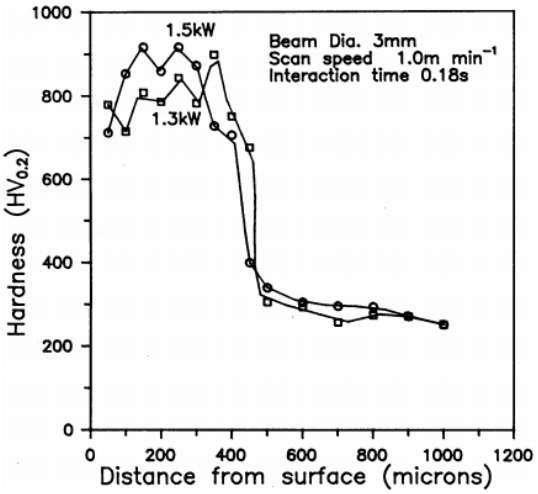

(b) Hardness profile of laser-hardened

Figure 2.16 Effect of laser surface hardening on AISI 5135 steel [9]

Milton Sergio Fernandes de Limaa et al (2007) [10] using a 2 kW fiber laser and an adapted linear axis for applies an automotive shaft was surface-remelted and hardened whose rotating axis produced helical tracks at 120 RPM. The process variable was the laser power, ranging from 300 to 1100 W with 1.9 mm beam diameter, which produced two regions in the material, a martensitic region (MR) and a partially transformed region (PTR). The MR is formed after rapid solidification or austenitization followed by rapid cooling (10^7 K.s^{-1}). The PTR is composed of martensite, unchanged pearlite and proeutectoid ferrite. The maximum case depth was about 0.3 mm. The micro hardness inside the martensitic regions are at least double that of the base material, i.e. between 800 than 600 HV compared to 300 HV. Thermal simulations using a modified Rosenthal formalism help elucidate the phase transformation inside the material and show good agreement with experimental results. The experimental laser-steel absorptivity was measured; they ranged between 38 and 59 % depending on the laser power and the amount of liquid at the surface, conclusion of result present as Figure 2.17.

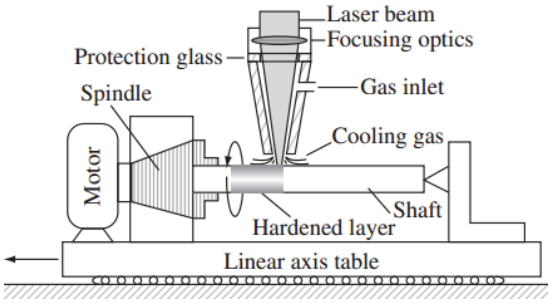

(a) Experimental diagram

Power (W)	Partially transformed region		Martensitic region	
	d_{PTR} (μm)	w_{PTR} (μm)	d_M (μm)	w_M (μm)
300	43	451	-	-
500	151	807	36	222
700	209	899	112	432
900	233	968	163	605
1100	369	1325	225	851

(b) Measurements of average depth and width of PTR and MR

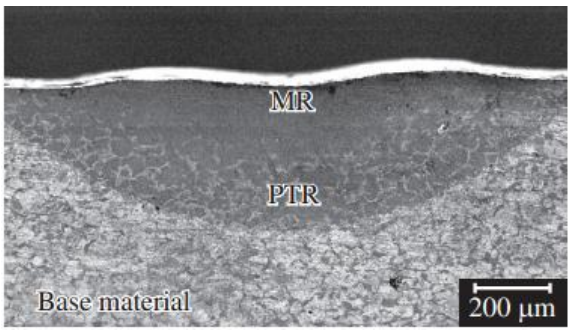

(c) Microstructure of hardened zone at 700 W

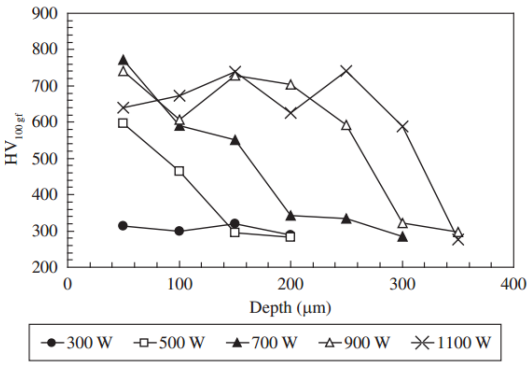

(d) Microhardness profile for depth

Figure 2.17 Laser surface hardening of an automotive shaft [10]

Yajun Fan et al (2007) [11] investigated about effect of phase transformations on mechanical behavior of AISI 1010 steel in laser forming. AISI 1010 steel plates were laser scanned straight along the center line under different conditions: 800 W and 50 mm/s and 400 W and 25 mm/s, maintaining laser spot size 4 mm diameter, and laser absorption by graphite coating. One of interesting results of experiments is the volume fraction of phase transformation at the end of heating and after cooling as shown in Figure 2.18 which indicated austenite and martensite transformation of low carbon steel such AISI 1010.

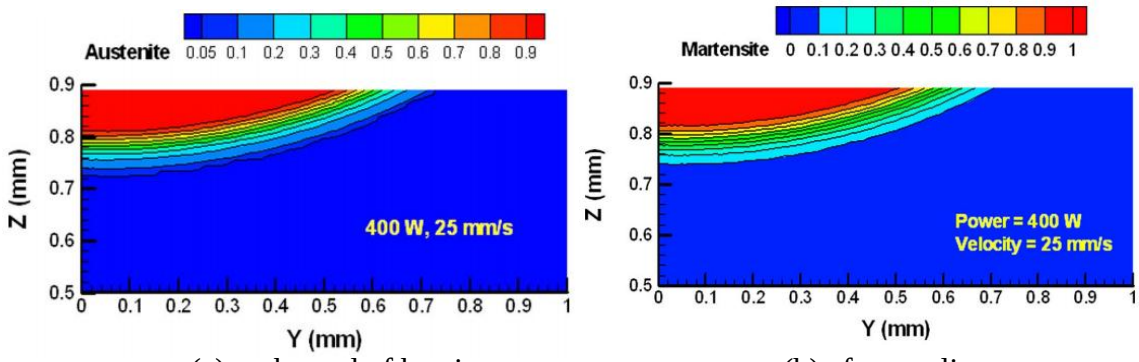

(a) at the end of heating (b) after cooling

Figure 2.18 The volume fraction of phase transformation [11]

A. Hussain et al (2007) [12] performed laser surface alloying of low carbon steel (AISI 1010) electroplated with thin 10 µm Ni using an 850 W CO_2 laser with travelling speed from 0.5 to 5 m/min and laser beam diameter 0.6 mm. The results of microhardness of the base metal was 125 HV, the hardness of the melted zones was measured in the range of 360 to 420 HV with maximum of the hardness at travelling speed 0.5 m/min as shown in Figure 2.19.

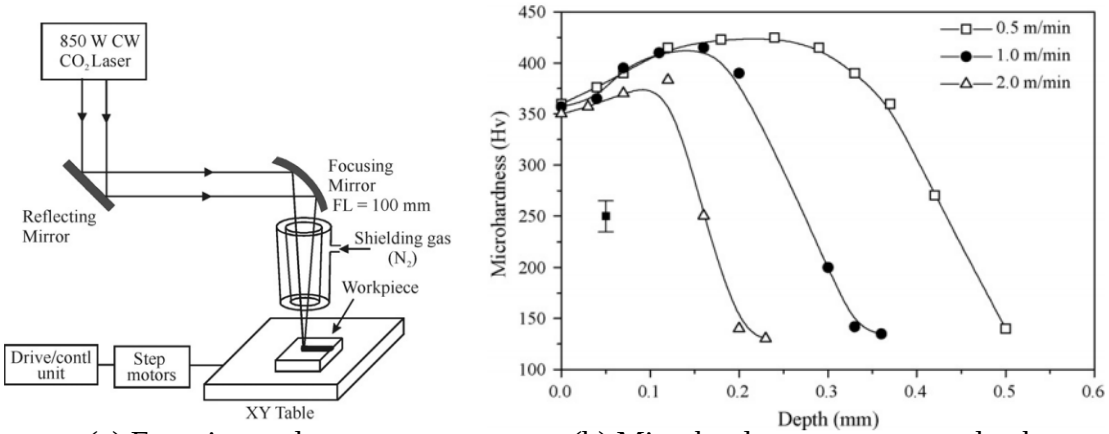

(a) Experimental setup (b) Microhardness versus case depth

Figure 2.19 Laser surface hardening of AISI 1010 by using an 850W CO_2 laser [12]

Ritesh S. Lakhkar et al (2007) [13] studied about laser hardening of AISI 4140 steel by focused on the development of a numerical model to predict the back tempering in multi-track laser hardening. A tempering model was combined with existing models of thermal behavior and phase change kinetics, which were developed earlier in the authors' group, to predict three-dimensional hardness profiles after multiple track laser hardening. The combined model was first validated through multi-track laser hardening tests and then used to predict and optimize the laser hardened case depth in multi-track laser hardening of AISI 4140 steel. The predictions and parameters optimized to obtain maximum case depth with the least variation along width of the hardened zone were experimentally verified. Case depths up to 2 mm were obtained with 5 mm overlapping of laser tracks as presents in Figure 2.20.

Property	Value
Pre-exponential (carbon in ferrite), $D_0\alpha$	6×10^{-5} m^2/s
Pre-exponential (carbon in austenite), $D_0\gamma$	1×10^{-5} m^2/s
Activation energy (ferrite), Q_α	80 kJ/mol
Activation energy (austenite), Q_γ	135 kJ/mol
Universal gas constant, R	8.314 J/molK
Pearlite grain spacing, λ	0.5 μm
Diameter of pearlite grain, L	8.85 μm
Average grain size, g	13.6 μm
Volume fraction of pearlite, f	0.45
Critical carbon content value, C_c	0.05%
Activation Energy (martensite for tempering) Q	196.888 kJ/mol
Pre-exponential, n	0.109
K_0	51.111×10^8 s^{-1}
Maximum hardness of martensite, $H_{martensite}$	700.00 HV
Maximum hardness of ε-carbide, $H_{\varepsilon\text{-carbide}}$	600.00 HV
Maximum hardness of ferrite, $H_{ferrite}$	150.00 HV
Maximum hardness of cementite, $H_{cementite}$	400.00 HV

(a) Constants used in diffusion model

Test no.	Power (W)	Speed (mm/s)	Maximum temperature under laser spot (C)	Depth of hardened zone (mm)	Melting yes/no
1	1200	2	1431	[a]	Yes
2	1200	1	1457	[a]	Yes
3	1200	0.5	1610	[a]	Yes
4	1100	1	1344	[a]	Yes
5	1100	0.5	1477	[a]	Yes
6	1000	1	1448	NO[a]	Yes
7	950	0.4	1361	1.91	No
8	950	0.3	1389	1.91[b]	No[b]
9	900	0.4	1354	1.89	No
10	850	0.5	1331	1.91	No
11	850	0.45	1344	1.9	No
12	850	0.4	1351	1.86	No
13	800	0.4	1245	1.7	No
14	800	0.3	1203	1.8	No

[a] No hardened zone possible.
[b] Close to melting temperature.

(b) Simulation matrix for determination of maximum case depth

Figure 2.20 Predictive modeling of multi-track laser hardening of AISI 4140 steel [13]

Neil S. Bailey et al (2009) [14] performed laser hardening of AISI 4140 steel by using high power direct diode 4 kW. This laser has a rectangular beam profile with a size of 12×8 mm and was set to a power of 1 kW and travelling speed of 2 mm/s. The laser track coincides with the center of the workpiece, the shorter axis of the beam profile aligned with the direction of laser travel. A constant absorptivity is 0.68 % and results of hardness profile as shown in Figure 2.21.

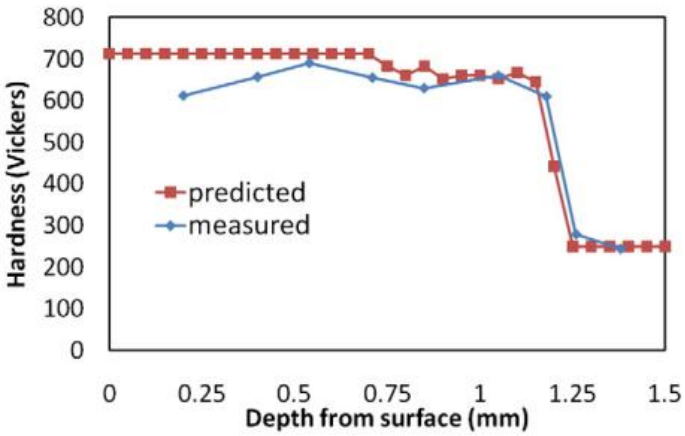

Figure 2.21 Comparison hardness of predicted and measured of AISI 4140 steel [14]

Flavia Aline Goia et al (2011) [15] was performed surface hardening of an AISI D6 cold work steel using a fiber Laser with x-y-z CNC table by single shot one second pulse time into 23 different regions and each region received a shot with a different laser power P and focal distance Z as Figure 2.22 (a). The overall absorptivity measured was about 37 % and the laser treatment produced two different zones: remelted and heat-affected. The surface layer was remelted and represented martensite and retained austenite phases. The region next to the free surface is composed of primary austenite dendrites with martensite plates with hardness between 400 and 500 HV. The heat-affect zone is composed of martensite, retained austenite, and carbides and has hardness up to 800 HV. The case depth in laser treated samples lies between 1 and 2 mm as shown in Figure 2.22 (b).

Shot	P (W)	Z (mm)	I (W/cm^2)	Melting (Y/N)	Hardness (HV) MZ	Hardness (HV) HAZ
1	100	+50	191	N	[a]	[a]
2	100	+30	529	N	[a]	[a]
3	300	+50	572	N	[a]	[a]
4	300	+50	572	N	[a]	[a]
5	200	+40	595	N	[a]	[a]
6	400	+50	762	N	[a]	[a]
7	300	+40	893	N	[a]	[a]
8	500	+50	953	N	[a]	[a]
9	200	+30	1058	N	[a]	[a]
10	600	+50	1143	Y	[a]	603 ± 30
11	400	+40	1191	Y	[a]	590 ± 60
12	700	+50	1334	Y	510 ± 40	600 ± 40
13	100	+18	1469	N	[a]	[a]
14	500	+40	1488	Y	620 ± 90	780 ± 50
15	800	+50	1524	Y	550 ± 20	550 ± 40
16	300	+30	1587	Y	660 ± 40	820 ± 90
17	900	+50	1715	Y	520 ± 10	560 ± 50
18	400	+30	2116	Y	570 ± 30	530 ± 20
19	500	+30	2645	Y	550 ± 20	430 ± 10
20	200	+18	2937	Y	580 ± 20	560 ± 40
21	300	+18	4406	Y	520 ± 20	470 ± 60
22	400	+18	5875	Y	550 ± 30	640 ± 70
23	500	+18	7343	Y	530 ± 10	520 ± 20

[a]Any interaction visible, with hardness similar to the base material, or too tiny to be measured.

(a) Single-shot laser parameters and results

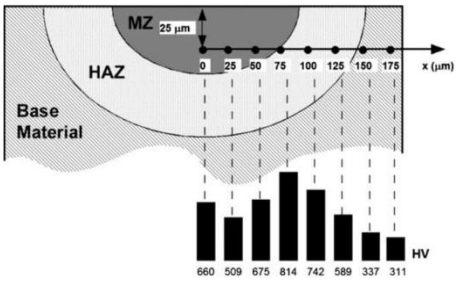

(b) Schematic picture of a cross section of shot 14 and the HV profile

Figure 2.22 Surface hardening of AISI D6 steel by using a fiber laser [15]

Mostly of the laser surface hardening applied by used the high power laser more than 400 W, the large laser beam diameter with the absorbent coating such as Mo_2S. Laser diode, CO_2 and fiber laser are popular laser type. Mostly of the hardness of AISI 4140 have about 700 HV with depth about 40% of the laser beam diameter and appeared melting zone when used too high power density of laser.

CHAPTER 3 EXPRERIMENTAL DESIGN AND SETUP

This chapter describes the experiment preparation, equipment, methodology, and procedure. The chapter is separated into three parts: The first part describes the equipment used for the laser hardening procedure, and the devices used for testing and analysis of the samples. The set-up and operation of the equipment is explained. The second part details the setting and performance testing of the laser. The third part explains the experimental procedure for each specimen: Sample preparation, parameter settings, and analysis scheme.

3.1 Experimental equipment

3.1.1 System overview

This study used laser system similar to that shown in Figure 3.1. The schematic diagram shows this laser system consisting of: A water-cooled CO_2 laser tube, a power supply, a control panel to adjust the power supply, current and voltage meters, a CNC system to control the movement of the beam, and reflective mirrors and a focusing lens to direct the beam toward the specimen. The specifications for this laser system are shown in Appendix E.

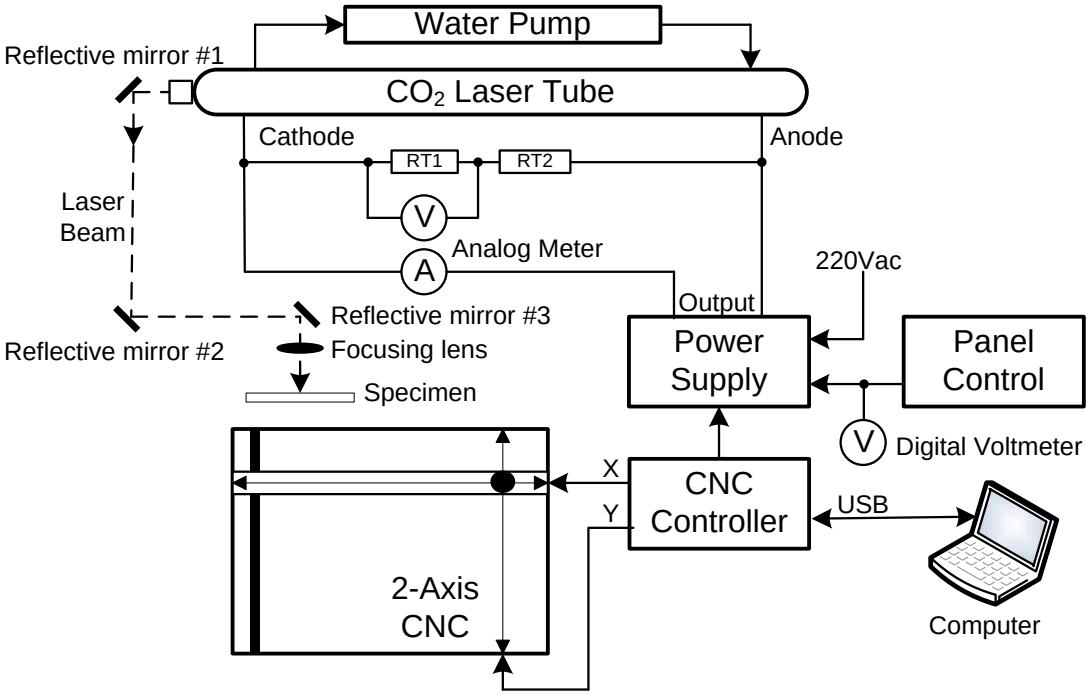

Figure 3.1 Block diagram of laser system

3.1.2 CO_2 laser tube

There are a variety of CO_2 lasers available on the market, varying in design complexity and processing technology. For this experiment a sealed CO_2 was chosen: Shown in Figure 3.2. This type of laser is common and readily available at a relatively low price. Main structures consist of: A hard borosilicate glass cylinder, a resonant cavity, and an electrode. The main cylinder is composed of three parts: The outer cylinder, an inner cylinder, and a water-cooling tube wrapped around the inner cylinder. The inner most cylinder functions as the discharge tube and contains a gas mixture of CO_2, N_2, and He. A water-cooling tube is wrapped around the discharge tube that allows water to be circulated from an adjacent reservoir for cooling. The outer cylinder functions as a resonant cavity with a reflecting mirror at one end and an output mirror at the other end. The reflecting mirror is made of optical glass with a gold film coating on the surface. The output mirror is made of Ge substrates with a dielectric multilayer film on the surface. The electrode section is a cylindrically shaped cathode with low sputtering and low gas absorption rate properties.

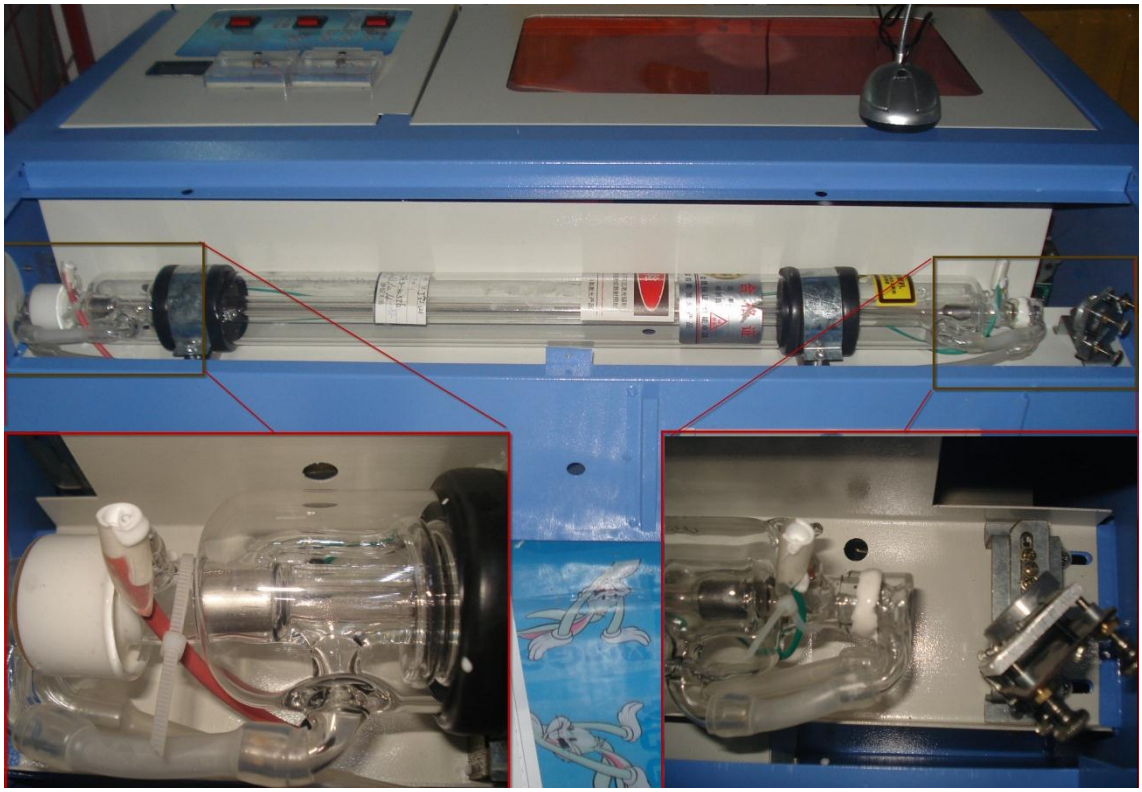

Figure 3.2 CO_2 laser tube

3.1.3 The power supply

The power supply functions as the pumping system, providing a high voltage, high frequency signal to the CO_2 laser tube to generate a sufficient power density. The power supply has an enable/disable function, and is able to receive a 0-5V DC signal sent from the control panel; subsequently allowing adjustments to the power density generated in the CO_2 laser tube.

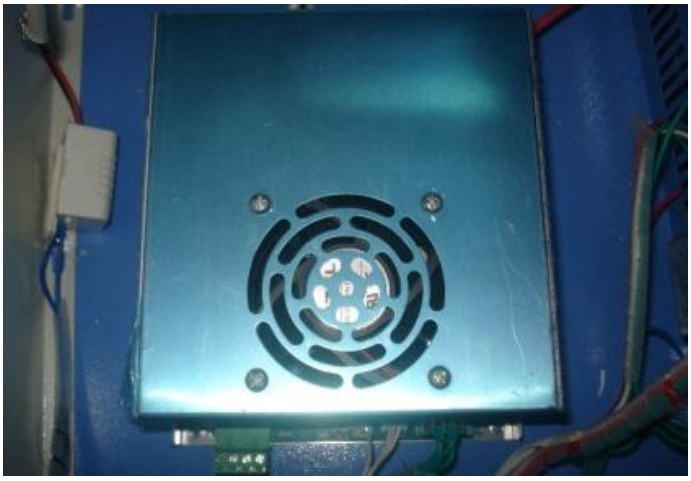

Figure 3.3 The power supply

3.1.4 The panel control

The control panel shown in Figure 3.4 allows the user to adjust the power density of the laser simply by setting laser power %. There are two analog meters to measure current and voltage sent to the laser, as well as a digital voltage meter measuring the input voltage sent from the control panel to the power supply. There is also a laser active on/off switch.

3.1.5 The current and voltage measuring

The current and voltage meters measure three important parameters necessary to measure the power density of the laser. An analog current meter measures the current in milliamps, taken at the cathode of the laser tube. An analog meter measures the voltage output of the power supply, taken at the anode of the laser tube, by way of a homemade 1000:1 voltage division ratio circuit. A digital meter displays the voltage output of the control panel being sent as an input signal to the power supply, depending on the laser power selection set by the operator.

Figure 3.4 Panel control and the current and voltage measuring

3.1.6 CNC system

A two axis CNC system controls the movement of the laser beam as shown in Figure 3.5, comprised two stepping motor drivers to allow for controlled movement along the X and Y access, an interface card shown in Figure 3.6 for interfacing between the motors and computer, and the necessary software to program the desired movement as shown in Figure 3.7.

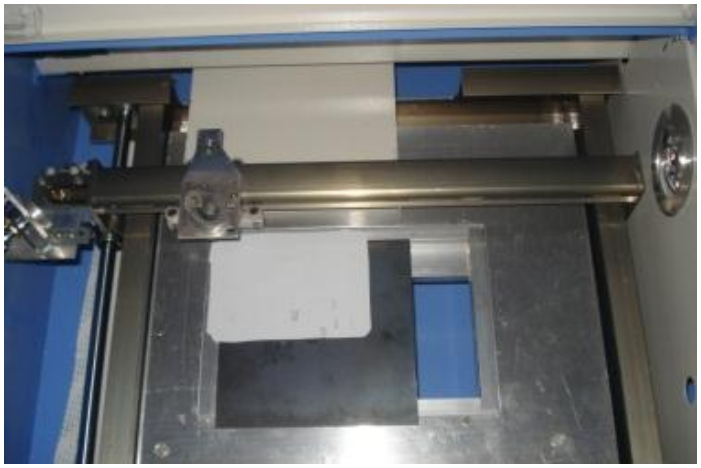

Figure 3.5 Two-axis CNC

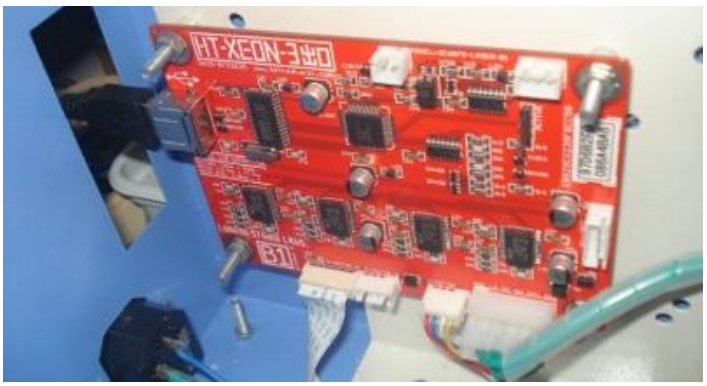

Figure 3.6 CNC controller

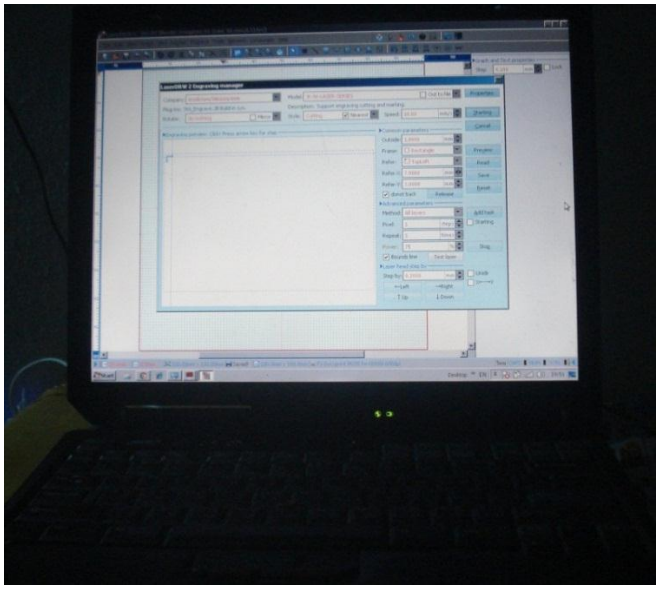

Figure 3.7 Computer and software control

3.1.7 Laser beam direction control

Three reflective mirrors and a focusing lens are required to direct the laser beam emanating from the laser tube to the precise spot on the workpiece as shown in Figure 3.8.

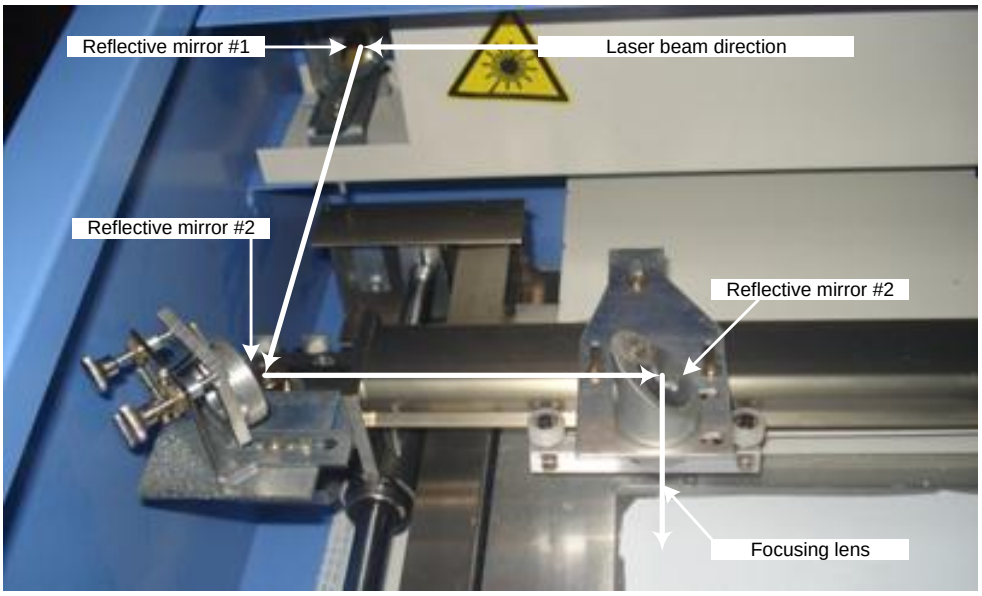

Figure 3.8 Reflective mirror and focusing lens

3.1.8 Microstructure analysis equipment

For microstructure analysis, the following set of equipment manufactured by Olympus was used: An GX51 inverted metallurgy microscope, a DP21 digital color camera with bright-field, dark-field, differential interference contrast (DIC), and simple polarization capabilities, and Olympus Stream software as shown in Figure 3.9.

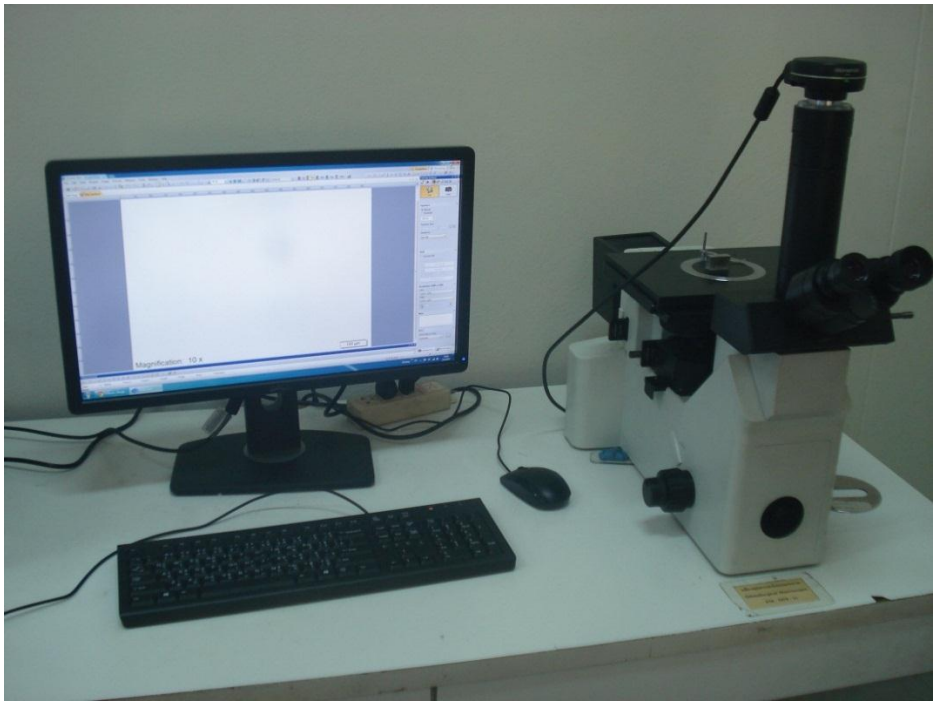

Figure 3.9 Microstructure analysis equipment

3.1.9 Micro-Vickers hardness tester

Hardness was tested mechanically using Micro-Vickers method, using the principle of pressing a rigid indenter into surface of the test specimen, then measuring the dimensions of the indentation. The surface of the material to be tested must be smooth. The micron-level dimensions of the indentation need to be measured with the aid of a microscope. Figure 3.10 shows the Micro-Vickers hardness tester model Innovatest 422D for using this research.

Figure 3.10 Micro-Vickers hardness tester model Innovatest 422D

3.1.10 Scanning Electron Microscope (SEM)

SEM is a tool to study the morphology of materials at the micro level, which is a very small detail because of the limitations of optical microscopy with wavelength larger than the characteristic morphology of some species are studied. The resolution of the conventional optical microscope is about 0.2 microns at the maximum magnification of 3000x. To view morphology details smaller than this, particularly to obtain an image with good contrast to separate these details SEM was used. The high magnification and short wavelength of SEM allows for a more detailed analysis of the morphology of the specimen. Figure 3.11 shows the JEOL SEM model SM-540V with a magnification ability of 15x to 200,000x, and a resolution of about 3.5nm.

Figure 3.11 SEM JEOL model JSM-5401LV

3.1.11 Flat black color spray

In Figure 3.12, "Leyland" brand flat black color spray paint is an all-purpose aerosol lacquer spray for multipurpose applications. A chemical composition and further specifications are not listed on the label but it is black color thus there is a mixture of high carbon concentration.

Figure 3.12 "Leyland" flat black color spray

3.2 Performance testing of the laser system

The laser system used for this experiment is not a high performance laser system built for a specific purpose. The limitations of the CO_2 laser system need to be determined, and the laser system needs to be performance testing to suit the specific requirements for this experiment.

3.2.1 Laser beam profile intensity distribution

The shape of the laser beam profile and intensity distribution was examined by directing the laser at an acrylic sheet. Figure 3.13 (a) shows the beam profile at the output tube. The power laser setting at the control panel was 15 %, beam diameter 3.5 mm, yielding a power density of 76 W/cm^2. The beam was directed to a clear acrylic sheet for one second. Figure 3.13 (b) shows the beam profile at the focus point. Power laser setting is 15 %, beam diameter is 0.2 mm, and the power density was calculated to be 18,023 W/cm^2. The beam was directed at a 10 mm/s travelling speed to a white acrylic sheet. Figure 3.13 (c) shows the beam profile at the focus point with the same settings as (b): power laser setting 15 %, 0.2 mm beam diameter, and power density 18,023 W/cm^2. The beam was directed at a clear acrylic sheet for about 10 seconds until the shape of the profile did not change. Considering the relationship between power density and beam diameter, a larger beam diameter will cause a profile with a flatter slope, a smaller beam diameter will cause a profile with a steeper slope. This infers, a larger beam diameter would be appropriate for heat treatment work, and a small beam diameter would be appropriate for cutting work.

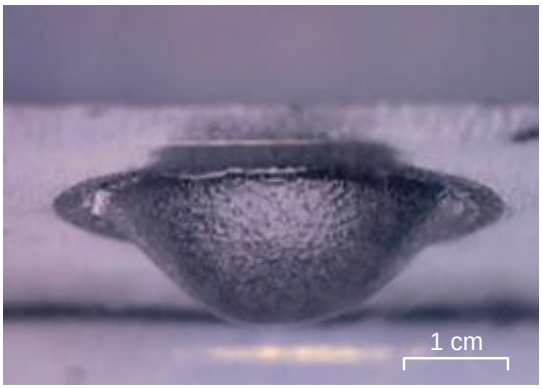

(a) At laser tube output

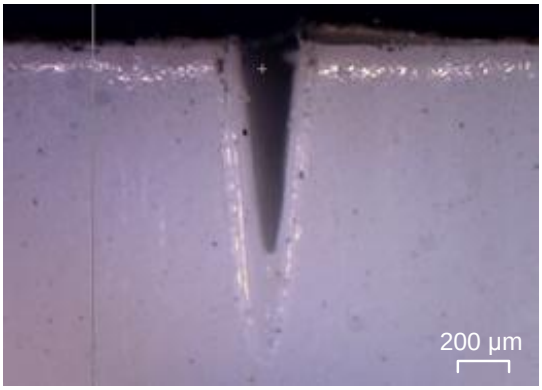

(b) At focus point

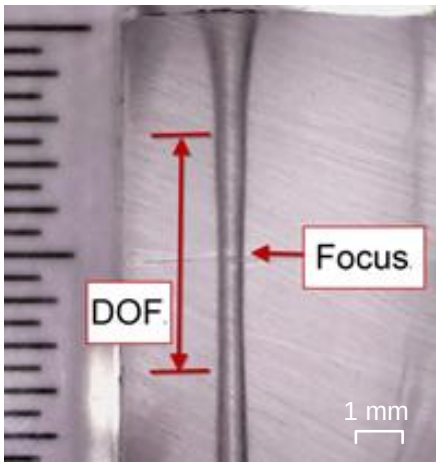

(c) DOF at focus point

Figure 3.13 Beam profile and DOF at laser tube output and at focus point

3.2.2 Depth of field (DOF)

Figure 3.13 (c) illustrates the DOF principle for the laser beam. This shows the range of distance from the focus point where the beam diameter remains steady. The DOF was calculated using equation 2.2 to be 5.686 mm.

3.2.3 Power density controlling

The correlation between the laser power setting at the control panel and the power density of the laser beam is shown in Table 3.13. For each laser power setting (%) the subsequent voltage and current was measured to determine output power. Additionally, the beam diameter was calculated from equation 2.1 to be 0.237 mm. The power density is calculated in (W/cm^2) at the tube and focus point.

Table 3.1 shows the maximum power output at the tube to be 36.4 W rather than the 40 W claimed in the specification. Furthermore, as the laser power setting are increased linearly over the 15 % to 90 % range, the resulting calculated power density is not linear.

This error is likely from reading the tube current from the analog meter. This error in power density was adjusted by a liner regression method. The linear regression equation is shown as equation 3.1. The results from Table 3.1 are plotted and shown as Figure 3.14, a graph, showing laser power setting (%) versus power density at the focus point (W/cm^2) based on measured values, and based on adjusted values.

Table 3.2 shows at laser power setting between 15 % and 90 %, the corresponding power density at the focus point calculated by measured values, and the adjusted value for power density at the focus point with linear regression adjustment.

Table 3.1 Current tube value related to power density and controlling

Laser Power Setting (%)	Voltage Control (V)	Current Tube (mA)	Power Output (W)	Power Density at tube (W/cm^2)	Power Density at focus (W/cm^2)
0	0	0	0.0	0	0
5	0	0	0.0	0	0
6	0.02	0	0.0	0	0
7	0.10	0	0.0	0	0
8	0.15	0	0.0	0	0
9	0.22	0	0.0	0	0
10	0.30	0.5	0.9	3	2,061
11	0.35	1	1.8	6	4,121
12	0.41	1.8	3.3	12	7,419
13	0.46	2.5	4.5	16	10,304
14	0.54	3.5	6.4	23	14,425
15	0.59	4	7.3	26	16,486
20	0.90	5	9.1	32	20,607
25	1.21	6	10.9	39	24,729
30	1.47	7	12.7	45	28,850
35	1.76	9	16.4	58	37,093
40	2.10	11	20.0	71	45,336
45	2.33	12.5	22.7	80	51,518
50	2.68	14	25.5	90	57,700
55	2.84	15	27.3	96	61,822
60	3.02	16	29.1	103	65,943
65	3.25	16.5	30.0	106	68,004
70	3.46	17	30.9	109	70,065
75	3.57	18	32.7	116	74,186
80	3.73	8.5	33.6	119	76,247
85	3.95	19	34.5	122	78,308
90	4.17	20	36.4	129	82,429
95	4.40	20	36.4	129	82,429
99.9	4.75	20	36.4	129	82,429

Note:

$$Power\ Output\ (W) = \frac{Maximum\ of\ power\ laser\ (W)}{Maximum\ of\ Current\ Tube\ (mA)} \times Current\ Tube\ Value\ (mA)$$

$$Power\ Density\ \left(\frac{W}{cm^2}\right) = \frac{Power\ Output\ (W)}{Beam\ Area\ (cm^2)}$$

$$LPS\ (\%) = -4.22675679 + 0.00105621211 \times Power\ Density\left(\frac{W}{cm^2}\right) \quad (3.1)$$

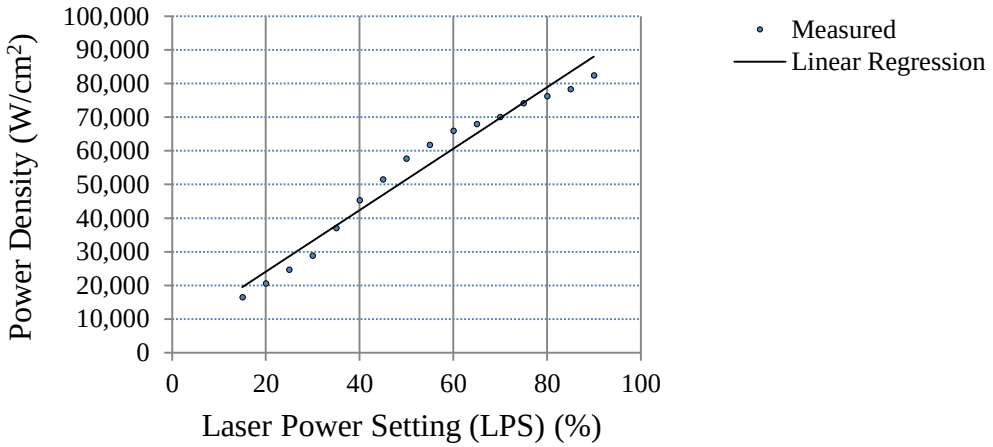

Figure 3.14 Relation of power density and power controlling

Table 3.2 Power density comparison by measured and linear regression

Setting laser power (%)	**Power Density by measured (W/cm^2)**	**Power Density by linear regression (W/cm^2)**
15	16,486	18,203
20	20,607	22,937
25	24,729	27,671
30	28,850	32,405
35	37,093	37,139
40	45,336	41,873
45	51,518	46,607
50	57,700	51,341
55	61,822	56,075
60	65,943	60,809
65	68,004	65,542
70	70,065	70,276
75	74,186	75,010
80	76,247	79,744
85	78,308	84,478
90	82,429	89,212

In addition, the control of this laser system is an open loop, rather than a closed loop control with positive feedback. There is no way for the control system of this laser to observe the processes and resulting power density that it is controlling. The power control stability of a closed loop system is higher than that of an open system.

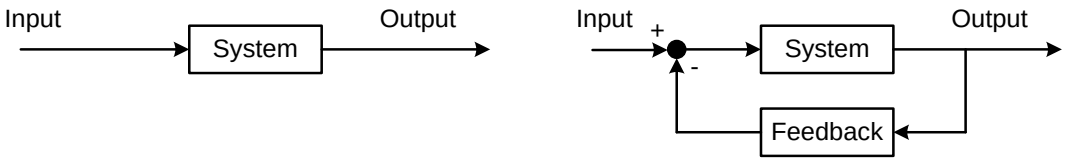

(a) Open loop control (b) Close loop control

Figure 3.15 Concept of control

3.2.4 Precision of movement

The movement of the CNC required calibration. The stepping of the CNC motors work by way of a pulse signal from the CNC controller to each phase of the stepping motor, initiating the timing for the precise fractional rotation of the motor for each step. The objective of the calibration is to examine the results of laser beam contact with a sample at different travel speeds.

Figure 3.16 and 3.17 is the top view of commercially pure Ti plate 0.5 mm grade 2 which there is chemical composition and mechanical properties as shown in Table 3.3, subjected to the laser beam at the focus point with a power density of 70,000 W/cm^2. The sample shown in Figure 3.16 had a travel speed set at 4 mm/s, while the sample shown in 3.17 had a travel speed of 2 mm/s.

The white circles in Figure 3.16 outline the observed step motion of the laser beam. Measured center to center there is a distance equal to 0.1 mm, which is the minimum of resolution ratio.

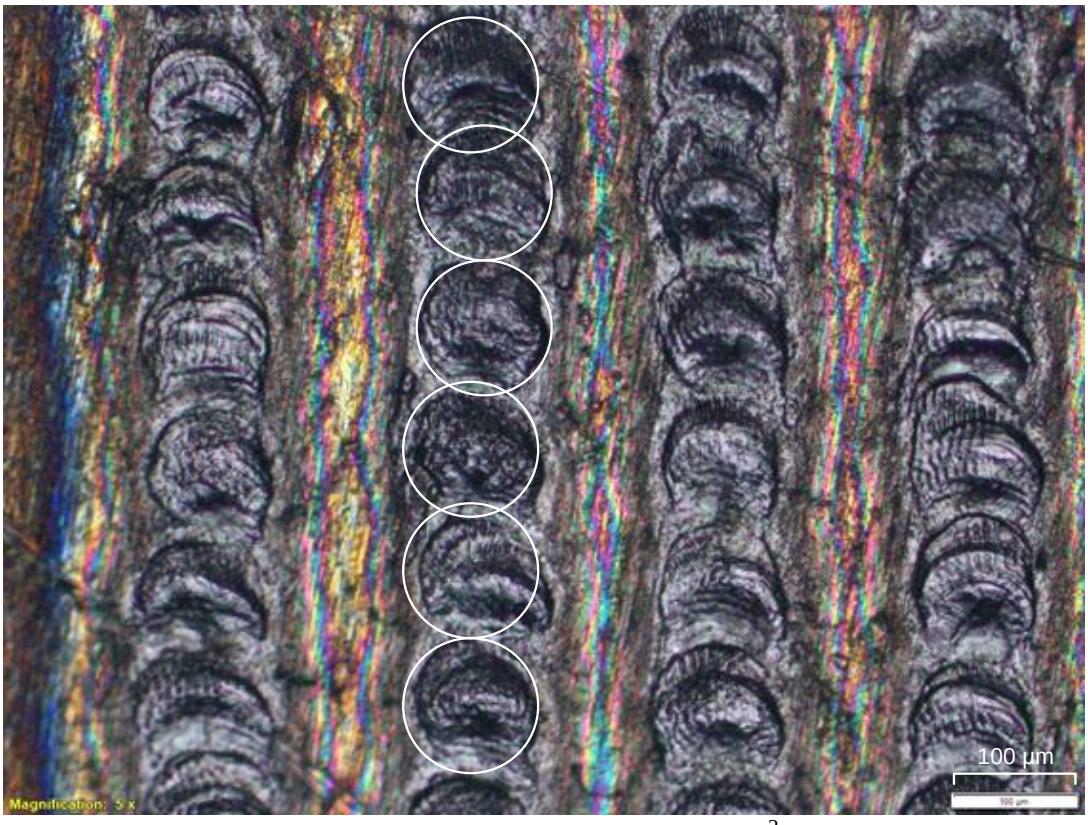

Figure 3.16 Top view of Ti at 70,000 W/cm^2, 4 mm/s

Figure 3.17 Top view of Ti at 70,000 W/cm^2, 2 mm/s

Table 3.3 Chemical composition and mechanical properties of CP Ti grade 2 [16]

Tensile Strength [MPa]	Elongation [%]	Reduction of area [%]	Chemical Composition (wt%)					
			C	Fe	H	N	O	Ti
344	20	35	0.1 max	0.3 max	0.015 max	0.03 max	0.25 max	99.2

3.2.5 Laser hammer

An interesting phenomenon was observed during the experiment that could best be described as "laser hammer" when the laser is switched on/off. Given the term "laser hammer" because the author thought it was somewhat analogous to the water hammer phenomena in piping; in the case where there is a shock pulse when the flow of water is turned on/off [17]. The principle similar, a high-density pulse occurs then the laser is turned on/off. Evidence of a high voltage signal from the power supply to the laser tube was detected and measured by a high voltage probe with an oscilloscope when the laser is turned on and off. Figure 3.18 shows the oscilloscope representation voltage anomaly when the laser is switched on/off, with the laser power setting at 15% and an expected power density of 18,203 W/cm^2. Figure 3.19 shows an OM image at the laser ending point where the laser was shut off, after contact with a Ti sheet, grade 2 of 0.5 mm thickness.

The high voltage signal at the anode of laser tube when laser is switched on will overshoot about 3 times of normal amplitude, and undershoots slightly when the laser is switched off. It is suspected that this anomaly originates from the on/off control but is not apparent in the soft start/stop control.

The advantage of laser hammer is that it improves absorbability from short burning at the surface when the laser is switched on; the disadvantages are surface defects from too high of a surface temperature.

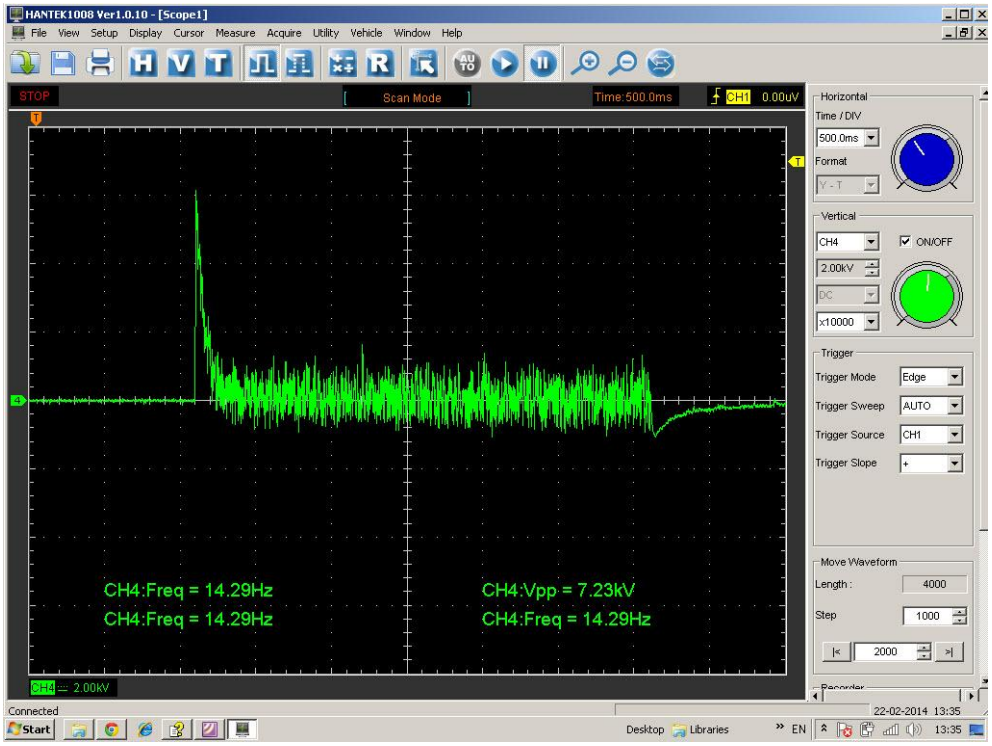

Figure 3.18 High voltage signal at the anode of laser tube

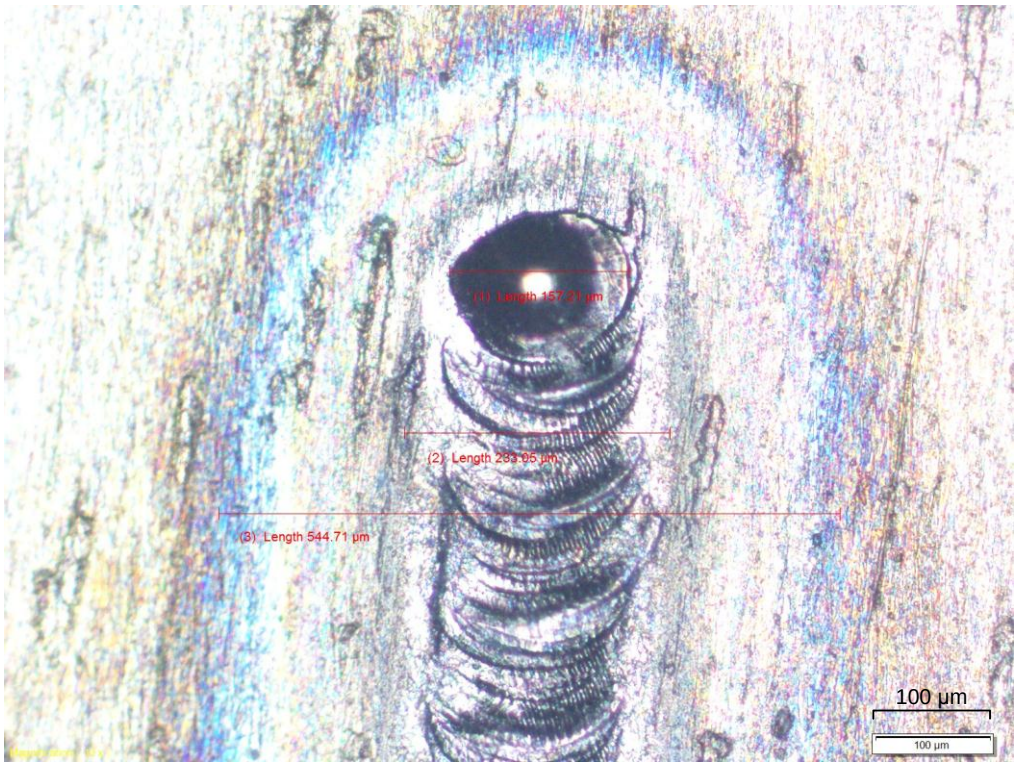

Figure 3.19 Laser ending point on Ti sheet grade 2, thickness 0.5 mm

3.3 Materials and methods

3.3.1 Workflow of tested specimens

Step of test as following order as shown in Figure 3.20 of each the specimens, starting from preparing the specimen, laser processing, and inspection by: OM for investigated the heat conduction of heat tint after the laser process and measured HAZ after the etching, SEM for investigated the microstructure, and HV for measured the surface hardening.

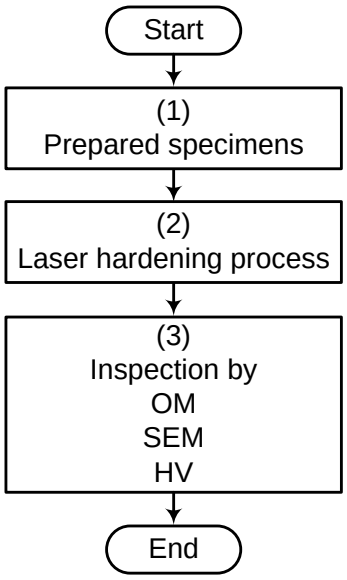

Figure 3.20 Workflow of tested specimens

3.3.2 Prepared specimens

Three general grades of low to medium carbon steel were selected for this experiment. Table 3.4 shows the chemical compositions of the specimens. Table 3.5 shows the mechanical properties of the specimens. Figure 3.21 shows an image of the three specimens. Various processing conditions were applied to each sample.

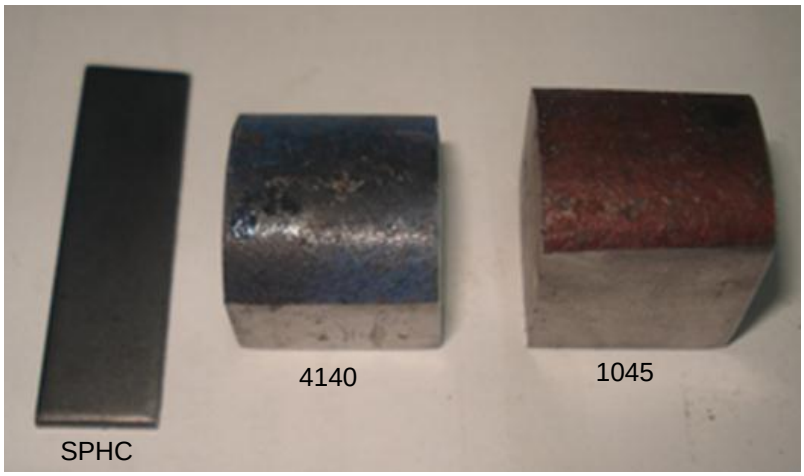

Figure 3.21 The specimens

Table 3.4 Chemical composition of the specimens [18]

Specimens Name	Grade	Chemical Composition (wt%)						
		C	Mn	P	S	Si	Cr	Mo
SPHC	SPHC	0.15 max	0.60 max	0.050 max	0.050 max	-	-	-
4140	AISI 4140	0.38-0.43	0.75-1.00	0.035 max	0.040 max	0.15-0.30	0.80-1.10	0.15-0.25
1045	AISI 1045	0.43-0.50	0.60-0.90	0.040 max	0.050 max	0.15-0.35	0.80-1.10	0.15-0.25

Table 3.5 Mechanical properties of the specimens [18]

Specimens Name	Tensile Strength [MPa]	Elongation [%]	Reduction of area [%]
SPHC	270	27	-
4140	1000-1200	11	45
1045	570-700	16	40

The SPHC steel is commonly known as “black steel”; it is hot rolled mild steel plate in accordance with Japanese Industrial Standards “JIS G3131: Hot-rolled mild steel plates, sheets and strip”. SPHC is generally used in forming work, presumably because it is easy to form.

The 4140 steel is commonly known as “blue steel”. It is medium hardenability, general purpose and high-tensile steel with used extensively in industry for a wide range of applications.

The 1045 steel is commonly known as “red steel”. It is a medium tensile, low hardenability carbon steel, generally supplied in the black hot rolled or occasionally in the normalized condition. It is further characterized by fairly good strength and impact properties, plus good machinability and reasonable weldability in the hot rolled or normalized condition. It is widely used in industrial applications requiring more wear resistance and strength.

Preparing the specimen for the experiment:
The 1.5 mm SPHC plate was cut with a hydraulic shearing machine to the following dimensions: 40 mm x 10 mm x 1.5 mm. The cutting side was ground with 100, 320, 600 and 1000 grit sandpaper for decreasing roughness. The 4140 and 1045 steel rod with the diameter of 2.54 mm was cut with a cold cutting machine to the dimensions of: 17 mm x 17 mm x 20 m. The cut side was ground with 100 grit sandpaper. The surface of the specimen was cleaned thoroughly until free from rust, dirt and grease. Primer was applied to only the 1045 and 4140 specimen, and then sprays painted with the “Leyland” brand flat black paint (color F-14) as shown in Figure 3.12 to a thickness of about 60 micron, and let dry for 2 hours.

Prior to the experiment the following assumptions were made:
Absorbability of the SPHC would be sufficient without coating because of the existing black surface. Reflectivity of the 4140 and 1045 steel are high and would need to be painted because of the existing surface was ground and polished. Both assumptions are supported by Figure 2.10.

The surface hardening may not be effective because of the low carbon content of the SPHC steel. Need to know results of relation of the laser power density with HAZ for guide line to heat conduction analysis. The surface hardening of the 4140 and 1045 steel is expected to be effective because of the carbon content of both steel and success by other research. Both assumptions are supported by Figure 2.3.

3.3.3 Laser process

The specimen was placed and the laser beam was applied at the focus point with layout plan of laser scan as shown in Figure 3.22, and was subjected to four laser power setting, and four travelling speeds for comparison and analysis.

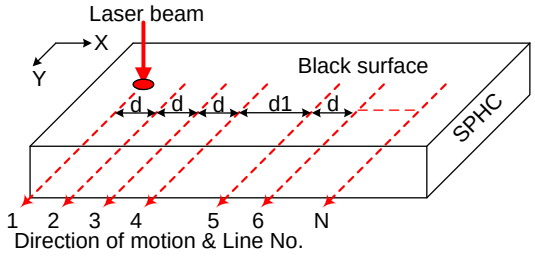

(a) SPHC

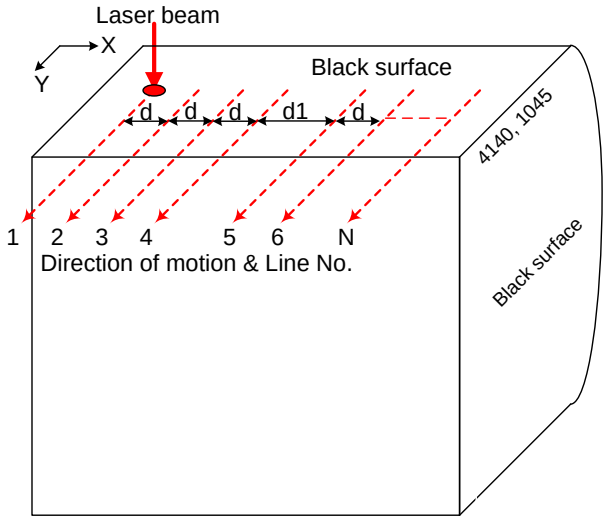

(b) 4140 & 1045

Figure 3.22 Layout plan of laser scan

Laser power setting and travelling speed as beam is applied to the SPHC specimen:
Four laser power setting were used: 15 %, 40 %, 65 %, and 90 %. The laser power setting correspond to beam density shown in Table 3.2. For each laser power setting four lines were created using a distinct travel speed: 1 mm/s, 2.5 mm/s, 5 mm/s, and 10 mm/s. The lines were equidistant at 1 mm. This scheme is listed in tabular form in Table 3.6.

Table 3.6 Process parameter for the SPHC steel, d = 1 mm, d1 = 2 mm

Line No.	Laser power setting (%)	Power Density (W/cm^2)	Travelling speed (mm/s)
1	15	18,203	1
2			2.5
3			5
4			10
5	40	41,873	1
6			2.5
7			5
8			10
9	65	65,542	1
10			2.5
11			5
12			10
13	90	89,212	1
14			2.5
15			5
16			10

Laser power setting, distance, and travelling speed as beam is applied to the 4140 and 1045 specimens: Two process parameters were set for the 4140 specimen. The first set of parameters applies the laser at four laser power setting: 16.9 %, 38 %, 59.1 %, and 80.2 %; this corresponds to expected power density at the laser beam focus point as: 20,000 W/cm^2, 40,000 W/cm^2, 60,000 W/cm^2, and 80,000 W/cm^2, respectively. For each set point, and corresponding power density, 16 lines were made separated at a distance of 0.5 mm. The 16 line sets are further subdivided into four travelling speeds: 1 mm/s, 2 mm/s, 4 mm/s, and 8 mm/s; such that lines 1-4 are separated by a distance of 0.5 mm and are subjected to the laser with a travelling speed of 1 mm/s, lines 5-8 again are separated by a distance of 1 mm and are subjected to the laser with a travelling speed of 2 mm/s, and so on. Each set of 16 lines subjected to the same power density, are separated by the next set of 16 lines with a different specific power density by a distance of 2 mm. This is perhaps better explained in tabular form as seen in Table 3.7.

The second process parameter is similar. The notable difference is the set point and corresponding expected power density and distance between the lines. For the second trial to the 4140 and 1045 specimen, four set points are used: 38 %, 59.1 %, 69.7 %, and 80.2 %; corresponding to an expected laser beam density at the focus point of: 40,000 W/cm^2, 60,000 W/cm^2, 70,000 W/cm^2, and 80,000 W/cm^2, respectively. Another difference for the second process parameter is the space in between the lines. There are 16 lines for each set point. Each set point has four distinct associated travel speeds: 1 mm/s, 2 mm/s, 4 mm/s, and 8 mm/s. Thus for a particular set point, lines 1 through 4 are subjected to the same travel speed. The lines 1 through 4 for the second set of parameters are a distance of 0.2 mm apart 1.4 mm away from the first subset of lines (1 through 4) are next subset of four lines (lines 5 through 8) subjected to a different travel speed. Lines 5 through 8 are 0.2 mm apart from one another, then a 1.4 mm distance, to another set of lines 9 through 12 separated by 0.2 mm then another 1.4 mm distance to the next set of four lines and so on. This scheme is represented in tabular form in Table 3.8.

Table 3.7 Process parameter set #1 for the 4140 steel, d = 0.5 mm, d1 = 1 mm

Line No.	Laser power setting (%)	Power Density (W/cm^2)	Travelling Speed (mm/s)
1-4	16.9	20,000	1
5-8			2
9-12			4
13-16			8
17-20	38.0	40,000	1
21-24			2
25-28			4
29-32			8
33-36	59.1	60,000	1
37-40			2
41-44			4
45-48			8
49-52	80.2	80,000	1
53-56			2
57-60			4
61-64			8

Table 3.8 Process parameter set #2 for the 4140 and 1045 steels, d=0.2 mm, d1=1.4 mm

Line No.	Laser power setting (%)	Power Density (W/cm^2)	Travelling Speed (mm/s)
1-4	38.0	40,000	1
5-8			2
9-12			4
13-16			8
17-20	59.1	60,000	1
21-24			2
25-28			4
29-32			8
33-36	69.7	70,000	1
37-40			2
41-44			4
45-48			8
49-52	80.2	80,000	1
53-56			2
57-60			4
61-64			8

3.3.4 Inspection by OM, SEM and HV

After the laser process, surface of specimen was examined by OM model Olympus GX51 inverted metallurgy microscope with Olympus Stream software for investigated the effect from the laser beam especially the heat conduction or the heat tint, then to the step of polishing and etching process.

The polishing and etching process, the specimen was then prepared for the microstructure inspection in accordance with the applicable ASTM and industry standards to better reveal the microstructure by casted with the clear resin in a circle

block. The cross section side was ground with 180, 320, 400, 600, 800, 1000, and 1200 grit sandpaper, then was polished with alumina powder, 0.3 microns in size for 40 minutes or until no lines were showing. The specimen was then etched with 2 % Nital, rinsed alcohol, and dried with a hot air blower.

After polishing and etching process, the specimen was examined second time with OM, and changes in the microstructure were noted, the width and depth of HAZ was recorded, then was examined third time for the microstructure analysis by using a SEM model JEOL JSM-5401LV. The final inspection consists of a mechanical hardness to determine the hardness value at each level of depth by using Micro-Vickers hardness tester model Innovatest 422D.

CHAPTER 4 RESULTS AND OPINIONS

4.1 The heat tint of the SPHC specimen

4.1.1 The heat tint

Before grinding and sanding, the surface removal and heat tint contour was observed. Figure 4.1 depicts this heat contour at a line with a set point of 90 %, a corresponding power density of 89,212 W/cm^2, with a travelling speed of 1mm/s. The resultant heat tint color is compared with the color chart Appendix F. It appears the heat tint color is outside the range of that for hardening, although it appears on the adjacent color chart for "low alloyed steel tempering".

The surface removal and heat tint contour were measured with respect to laser power density and travelling speed. The surface removal width (W_P) and depth (D_P), and heat tint width (W_F) and depth (D_F) were recorded with respect to line number, corresponding travelling speed, and laser power density, listed in Table 4.1. The width and depth of the heat tint contour (W_F and D_F) is observed as a violet and dark blue color; according to Appendix F corresponds to a temperature of (285°C). An example of the relationship between the surface removal and heat tint contour and the related dimensions is shown in Figure 4.1.

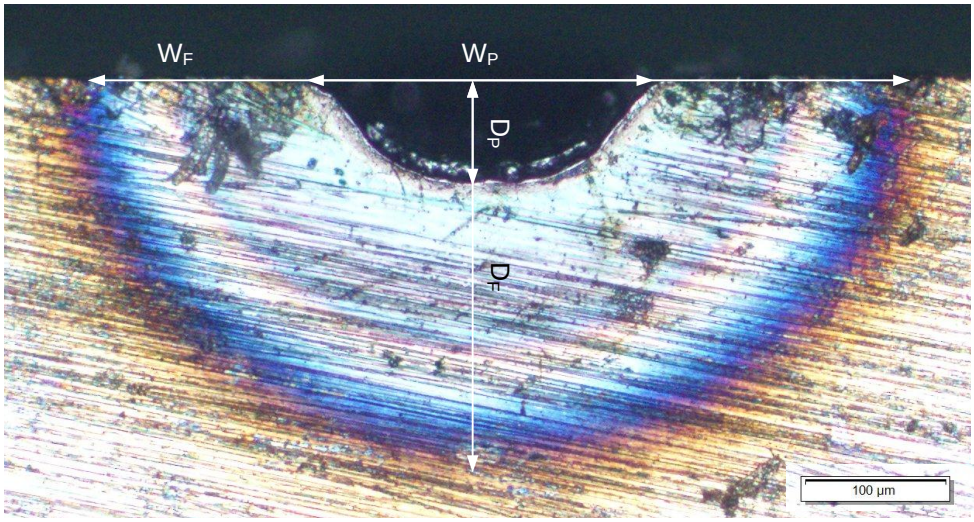

Figure 4.1 The surface removal and heat tint before grinding

Table 4.1 Dimension of the surface removal and heat tint

Line No.	Travelling Speed (mm/s)	Power Density (W/cm^2)	Width (µm)		Depth (µm)	
			W_F	W_P	D_F	D_P
1	1	18,203	0	0	0	0
5		41,837	312	174	127	42
9		65,873	503	228	227	69
13		89,212	597	240	263	75
2	2.5	18,203	0	0	0	0
6		41,837	303	157	119	43
10		65,873	414	208	175	61
14		89,212	449	234	191	48
3	5	18,203	0	0	0	0
7		41,837	260	122	106	34
11		65,873	363	171	148	48
15		89,212	395	188	167	44
4	10	18,203	0	0	0	0
8		41,837	230	90	81	19
12		65,873	319	132	127	24
16		89,212	366	158	151	32

4.1.2 Microstructure

After etching and upon a second inspection with an OM, no substantial changes in microstructure were observed. However, through the OM a faint line that delineates HAZ, and very small microstructure change were observed. This is shown in Figure 4.2.

Figure 4.2 Microstructure after etching

4.1.3 Opinions

1. Power and density affect the dimensions of surface removal and heat tint. The data from Table 4.1 is plotted. The dimensions of surface removal (W_P and D_P), versus laser power density, with respect to travelling speed are shown in Figure 4.3. The dimensions of heat tint (W_F and D_F), versus power density, with respect to travelling speed are shown in Figure 4.4.

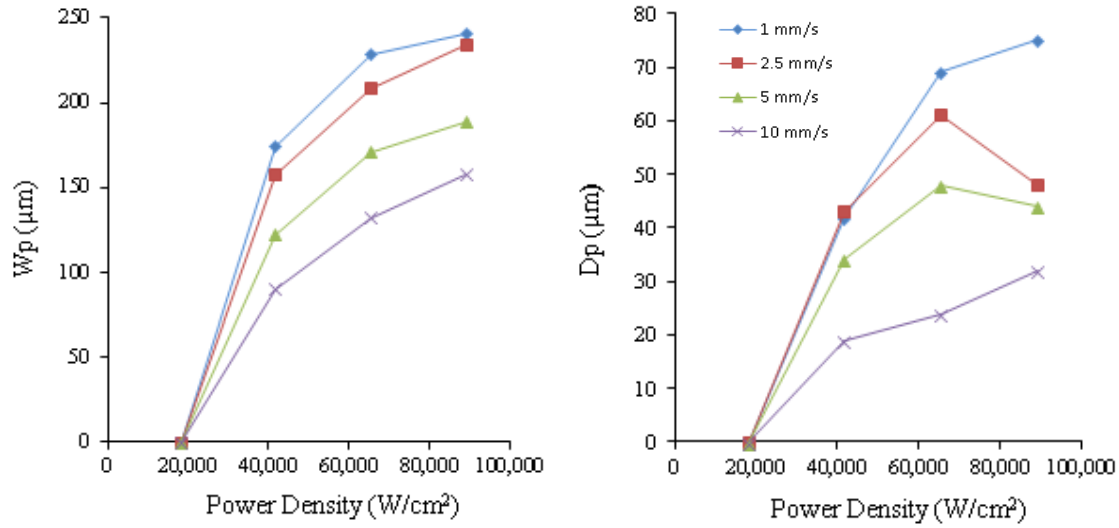

(a) Width of surface removal (b) Depth of surface removal

Figure 4.3 Relation of power density with surface removal of the SPHC specimen

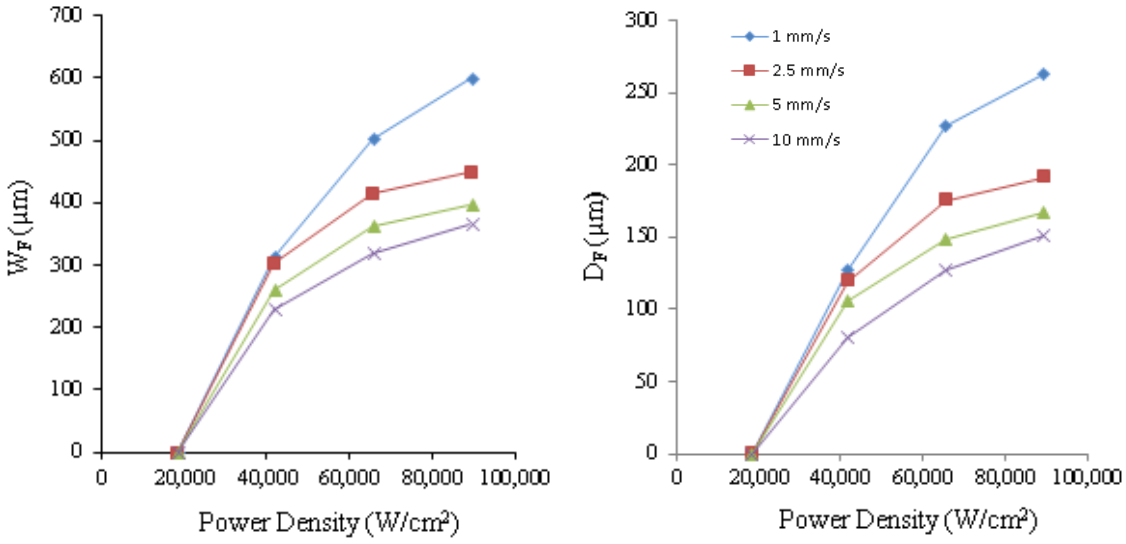

(a) Width of heat tint (b) Depth of heat tint

Figure 4.4 Relation of power density with heat tint at 285°C of the SPHC specimen

2. The was very little observed change of microstructure. This was possibly due to three reasons.

- The carbon content of SPHC may be too low. The carbon content of SPHC ranges from 0-0.15 % by weight. It is possible the carbon content of this sample is below 0.1 %, the minimum carbon content required for laser hardening (Figure 2.3).
- The observable changes in microstructure were lost due to surface removal, or lost during the grinding and polishing process.
- The region where microstructure changes had occurred is too small to be observed.

3. The black oxide at the surface of SPHC is good absorber caused absorptivity about 60-80 % (Figure 2.10) at surface. Without of the black oxide at the surface, absorptivity reduced to less than 10 %.

4.2 The surface hardening of the 4140 specimen

4.2.1 The heat tint

Before grinding and sanding, surface removal and a heat tint contour was observed similar to that of the SPHC sample.

4.2.2 HAZ dimensions

After etching there obvious changes to microstructure was observed with OM. Figure 4.5 shows HAZ of the sample subjected to the laser beam with a laser power setting of 59.1 % and a corresponding power density 40,000 W/cm^2, with travelling speed 2 mm/s. Observed measurements of the HAZ dimensions were taken for each combination of travelling speed respective laser beam power density. Table 4.2 is average value of observed HAZ dimensions of process parameter set #1 with surface removal less than 10 micron.

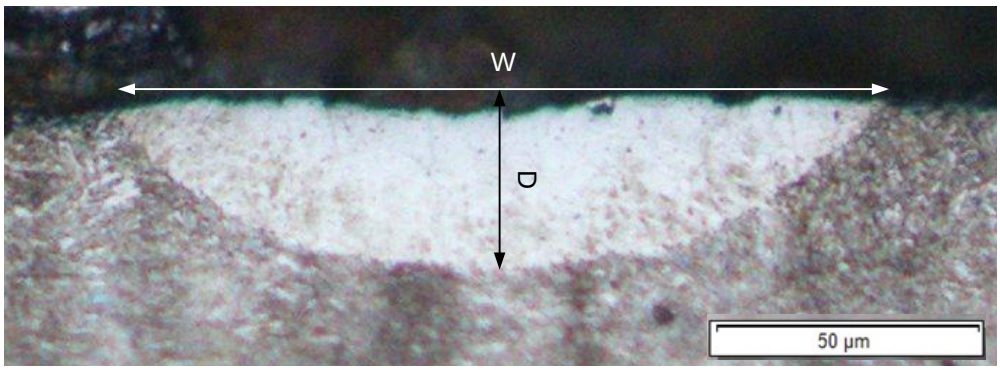

Figure 4.5 HAZ dimensions with 40,000 W/cm^2, 2 mm/s

Table 4.2 HAZ dimensions by laser process with following parameter #1

Line No.	Travelling Speed (mm/s)	Power Density (W/cm^2)	Width (µm) W	Depth (µm) D
1-4	1	20,000	0	0
17-20		40,000	142	25
33-36		60,000	218	45
49-52		80,000	239	69
5-8	2	20,000	0	0
21-24		40,000	138	28
37-40		60,000	183	40
53-56		80,000	241	58
9-12	4	20,000	0	0
25-28		40,000	156	35
41-44		60,000	169	35
57-60		80,000	152	32
13-16	8	20,000	0	0
29-32		40,000	171	38
45-48		60,000	175	32
61-64		80,000	174	39

For process parameter set #2: The laser beam diameter was 0.237mm and the distance in between the lines from center to center was 0.2 mm resulting in some overlap of HAZ as shown in Figure 4.6. Shown are images of the sample being subjected to the laser with a laser power setting of 69.7 %, corresponding to a power density of 70,000 W/cm^2, and a travelling speed of 4 mm/s with very little observed the surface removal.

Figure 4.6 Surface of laser hardened layer with 70,000 W/cm^2, 4 mm/s, d = 0.2 mm

For process parameter set two, the dimensions for HAZ and surface removal were averaged for each 4-line set with respect to the distinct power density and travelling speed. The results are shown in Table 4.3.

Table 4.3 HAZ dimensions by laser process with following parameter #2

Line No.	Travelling Speed (mm/s)	Power Density (W/cm^2)	HAZ		Removal
			Width (µm) W	Depth (µm) D	Depth (µm) D_C
1-4	1	40,000	171	36	10
17-20		60,000	252	109	30
33-36		70,000	236	81	6
49-52		80,000	265	82	20
5-8	2	40,000	163	36	7
21-24		60,000	272	103	23
37-40		70,000	261	94	10
53-56		80,000	257	70	6
9-12	4	40,000	137	30	3
25-28		60,000	263	94	8
41-44		70,000	268	104	0
57-60		80,000	252	84	0
13-16	8	40,000	145	28	0
29-32		60,000	242	75	0
45-48		70,000	252	91	0
61-64		80,000	217	49	0

Data from Table 4.2, representing parameter set #1 and data from Table 4.3, representing parameter set #2 are plotted with respect to depict the effect power density and travelling speed has on HAZ dimensions and surface removal.

In the case of process parameter set #1: HAZ dimensions of width and depth do not increase substantially for power density greater than 40,000 W/cm^2 and travelling speed greater than 4mm/s. Figure 4.7 represents the dimensions of HAZ width and depth, versus power density with respect to travelling speed for process parameter set #1.

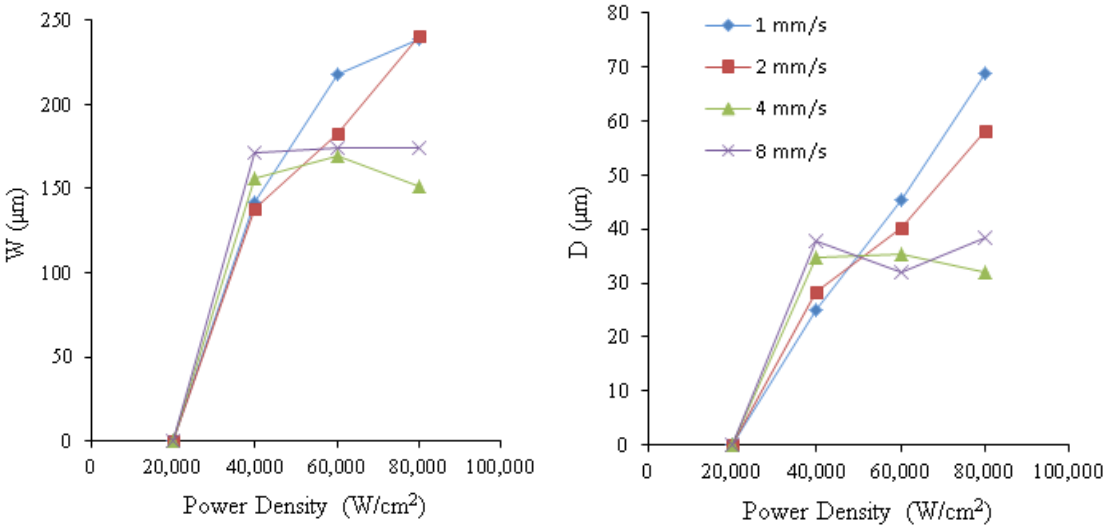

(a) Width of HAZ (b) Depth of HAZ

Figure 4.7 Relation of power density with HAZ of process parameter set #1

In the case of process parameter set #2: HAZ dimensions of width and depth decrease or are unstable for every travelling speed with a power density greater than 60,000 W/cm^2. Figure 4.8 represents the measurements of HAZ width and depth, versus power density with respect to travelling speed for process parameter set #2.

Figure 4.8 (c) shows, using process parameter set #2; for each travelling speed, the surface removal peaks at a power density of 60,000 W/cm^2 and then has a tendency to decrease.

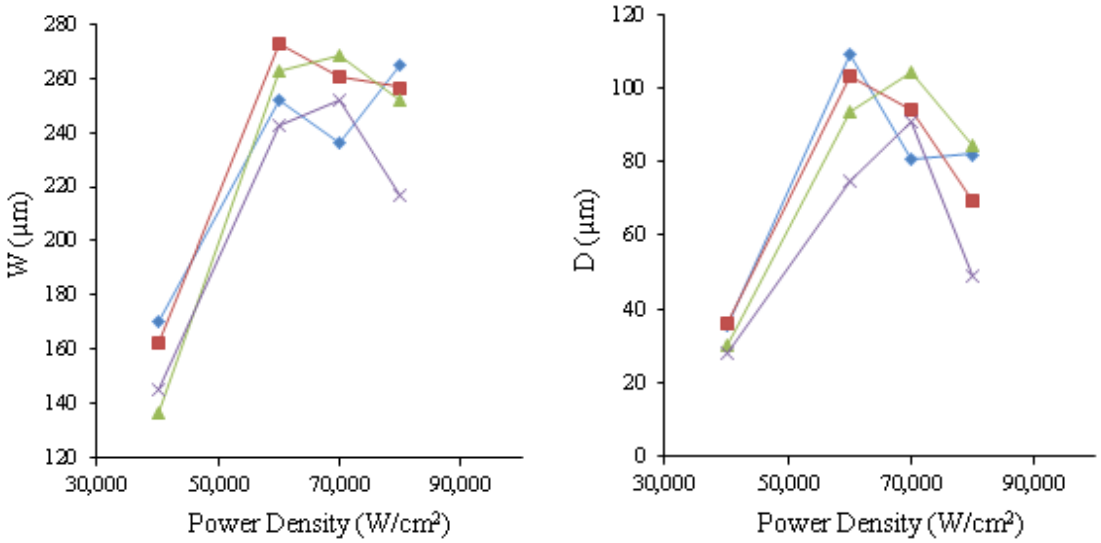

(a) Width of HAZ

(b) Depth of HAZ

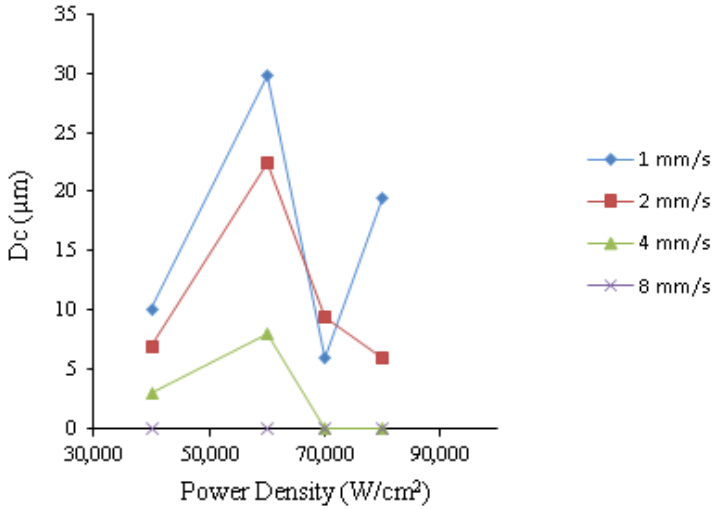

(c) Depth of the surface removal

Figure 4.8 Relation of power density with HAZ of process parameter set #2

4.2.3 Microstructure

The SEM was used to analyze the microstructure at the base and HAZ boundary for the 4140 specimen subjected to the laser beam at a power density of 70,000 W/cm^2, 4 mm/s, line distance of 0.2 mm (process parameter set #2). The experimental specimen was compared with a reference specimen: The reference specimen was cut from a hot rolled steel round bar, 25.4 mm diameter, austenitized at 845°C for 1 hour, and water quenched [18]. Under an SEM the reference specimen shows a fine grain micro-structure, like homogeneous, untempered martensite. The structure within the HAZ of the experimental specimen looks the same as the reference specimen as shown in Figure 4.9 (a), (b), (c) and (d). The black color circled in white is a particle of the flat black color spray paint as shown in Figure 4.9 (a) and (d).

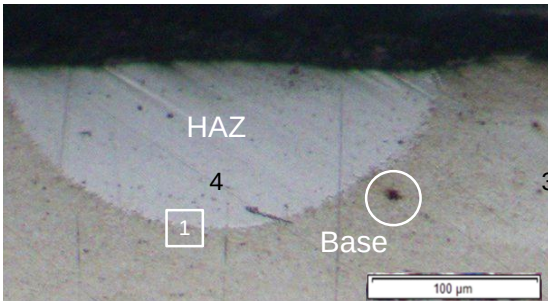

(a) Mapping point for SEM by OM

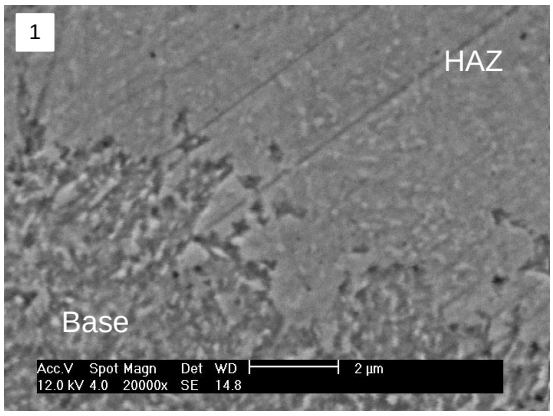

(b) SEM Magnification 20,000x

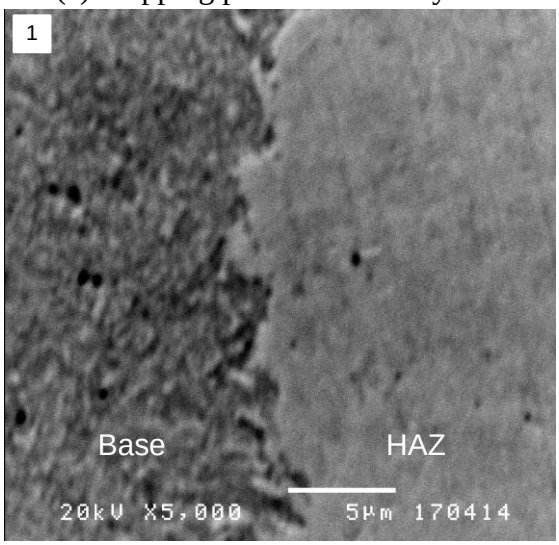

(c) SEM Magnification 5,000x

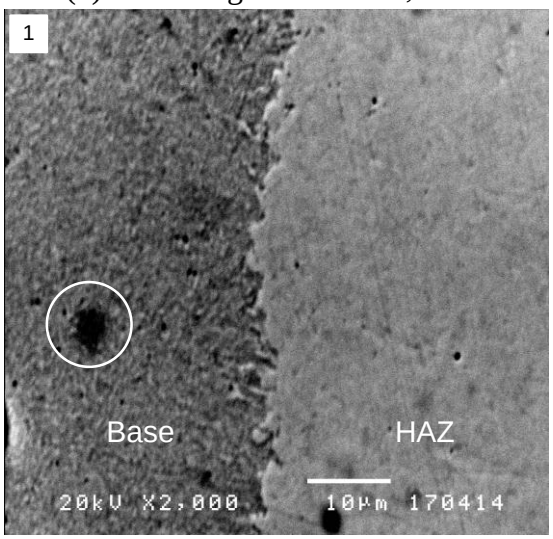

(d) SEM Magnification 2,000x

Figure 4.9 SEM of HAZ boundary of the 4140 specimen

4.2.4 Microhardness

A mechanical hardness test was performed on the 4140 specimen subjected to a laser power density of 70,000 W/cm^2, travelling speed 4 mm/s and distance 0.2 mm. Table 4.4 lists the results of from Micro-Vickers hardness tester, which refers to test point location shown in Figure 4.10. Table 4.4 shows dimensions of the indentation and hardness in units of HRC and HV. At a half of depth of HAZ, the hardness value about 700HV, which is twice the hard as the base steel.

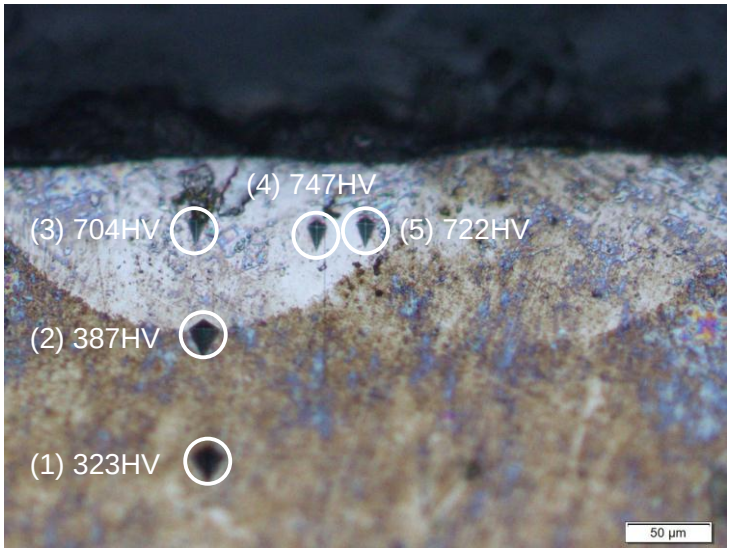

Figure 4.10 Measuring point of the 4140 specimen

Table 4.4 Hardness of the 4140 specimen by load 100 g, dwell 10 s

Point No.	D1(µm)	D2(µm)	HRC	HV
(1)	22.36	25.50	32.6	323.7
(2)	19.36	24.40	39.5	387.4
(3)	13.21	19.23	60.3	704.5
(4)	12.84	18.65	62.1	747.8
(5)	12.79	19.26	61.1	722.3

4.2.5 Opinions

1. The laser hardening process for the 4140 specimen was successful, except for the surface removal anomaly. The Micro-Vickers hardness test for a sample without significant surface removal achieved at half the HAV depth, a hardness value of 700HV which is twice as hard as the base steel.

2. The flat black color spray point improved absorbability, but became unstable and behaved unpredictably, especially in instances there the laser beam overlapped.

3. An additional trial was run, by having the laser beam overlap 50 %, with a 0.1 mm center-to-center distance between each line, a power density of 40,000 W/cm^2, and a travelling speed of 2 mm/s. As shown in Figure 4.11, by increasing the beam overlap, HAZ becomes increasingly irregular for each line and the surface removal is exacerbated.

Figure 4.11 Surface of laser hardened layer with 40,000 W/cm^2, 2 mm/s, d = 0.1 mm

4.3 The surface hardening of the 1045 specimen

4.3.1 The heat tint

Before grinding and sanding, surface removal and a heat tint contour was observed similar to that of the SPHC and 1045 specimens.

4.3.2 HAZ dimensions

After etching, the 1045 specimen was examined by the OM. Changes to the microstructure were observed. Figure 4.12 shows resulting HAZ to the 1045 specimen by the application of the laser at a power density of 40,000 W/cm^2 and 60,000 W/cm^2 respectively, both with travelling speed 2 mm/s. Measured values of HAZ and surface removal were taken for the specific beam power density and travelling speed. The average HAZ and surface removal measurements of each 4-line set with the same power density and travelling speed are listed in Table 4.5

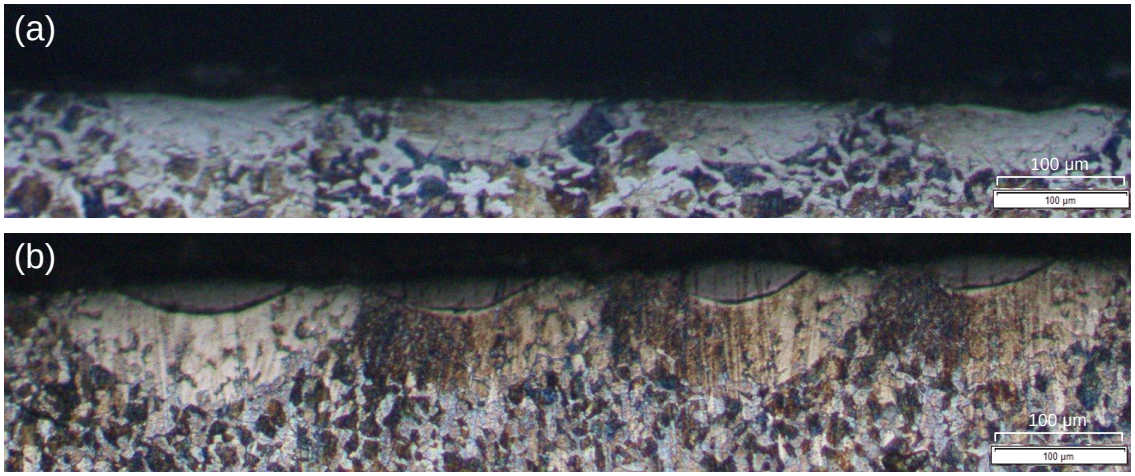

Figure 4.12 Surface of laser hardened layer of the 1045 specimen with: (a) 40,000 W/cm^2, 2 mm/s, d = 0.2 mm; (b) 60,000 W/cm^2, 2 mm/s, d = 0.2 mm

Table 4.5 HAZ dimensions by laser process of the 1045 specimen

Line No.	Travelling Speed (mm/s)	Power Density (W/cm^2)	HAZ		Removal
			Width (μm) W	Depth (μm) D	Depth (μm) D_C
1-4	1	40,000	181	50	9
17-20		60,000	237	90	37
33-36		70,000	223	81	16
49-52		80,000	244	91	20
5-8	2	40,000	172	49	5
21-24		60,000	234	94	24
37-40		70,000	238	87	12
53-56		80,000	227	79	9
9-12	4	40,000	151	44	3
25-28		60,000	206	67	6
41-44		70,000	220	76	2
57-60		80,000	238	78	0
13-16	8	40,000	176	51	0
29-32		60,000	171	54	0
45-48		70,000	205	66	0
61-64		80,000	226	83	0

Regarding the 1045 specimen, the results shown in Table 4.5 are plotted and shown in Figure 4.13. The graphs plot the measurements of HAZ and surface removal, versus laser beam power density with respect to travel time.

For travelling speeds less than 2 mm/s, the results follow a trend similar to that of the tested 4140 specimen; there is little increase of HAZ dimensions when a beam density of 60,000 W/cm^2 is applied.

For travelling speeds 4 mm/s and greater the dimensions of HAZ increase steadily with the increase of beam density.

Similar to the tested 4140 specimen, depth of surface removal peaks at a beam density of 60,000 W/cm^2 for all travelling speeds

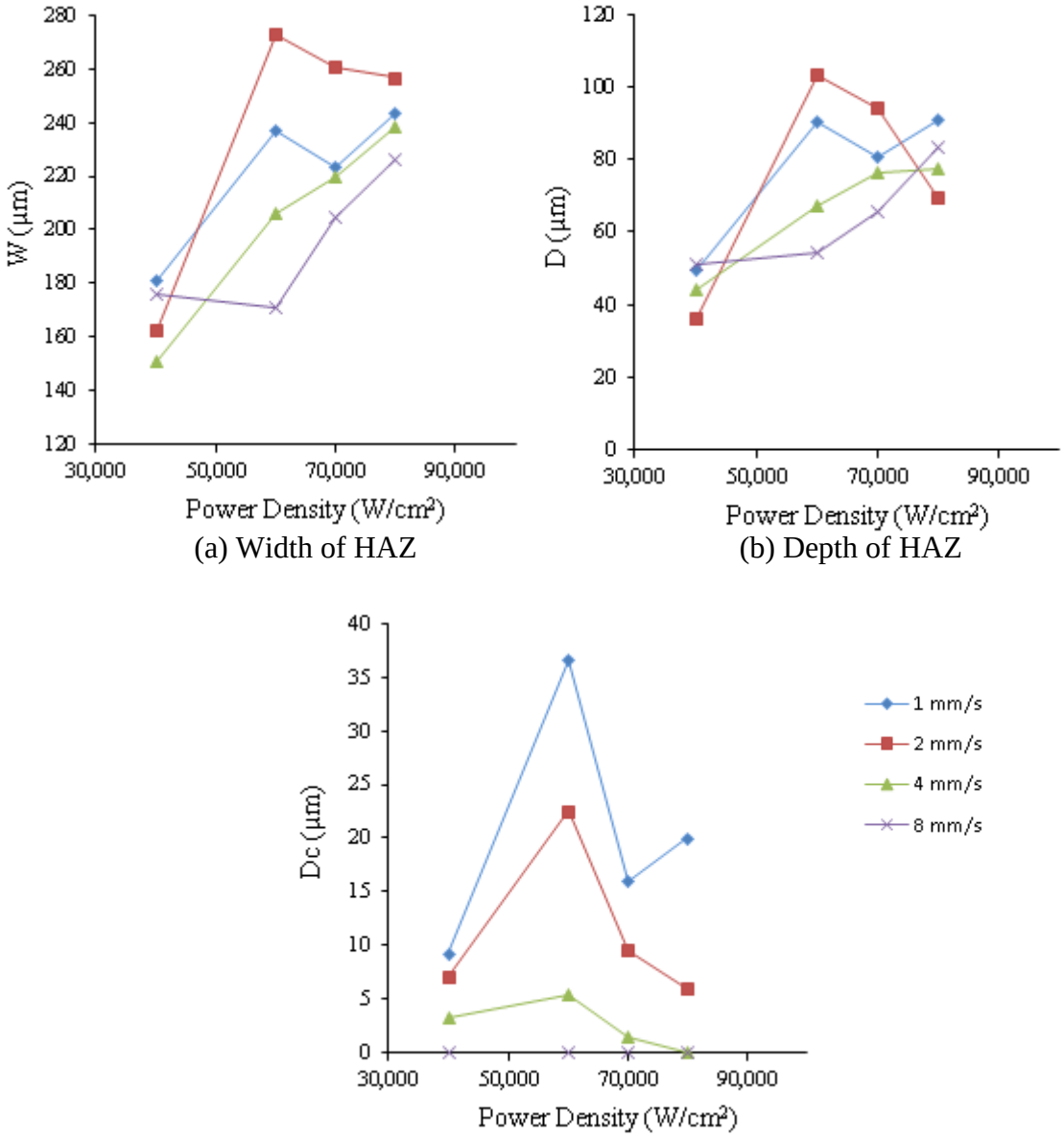

(a) Width of HAZ

(b) Depth of HAZ

(c) Depth of surface removal

Figure 4.13 Relation of power density with HAZ and surface removal of the 1045 steel

4.3.3 Microstructure

A sample of the 1045 specimen subjected to a beam density of 60,000 W/cm^2, a travelling speed of 2 mm/s, and a center-to-center line distance of 0.2 mm was prepared for examination of the microstructure at the base and HAZ boundary by the SEM. The experimental specimen was compared to a reference sample of similar material. The reference material was cut from a 25.4 mm diameter hot rolled steel bar that was austenitized at 845°C for 1 hour and air cooled. The structure of both the experimental specimen and the reference sample have a structure composed of fine lamellar perlite (dark) and ferrite (white) [18] as shown in Figure 4.14 (c) and (d). The image shown Figure 4.14 (a) and (b) are that of the base zone, HAZ and the removal zone (RZ) of the 1045 experimental specimen. The black particle encircled in white as shown in Figure 4.14 (a) is a particle of the flat black color spray paint.

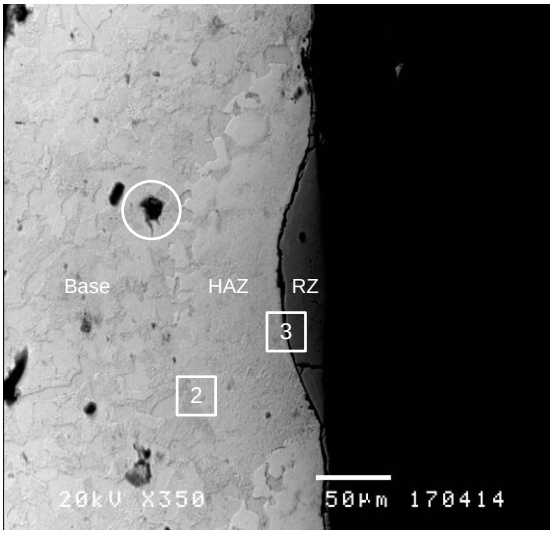

(a) Mapping point of SEM and EDS

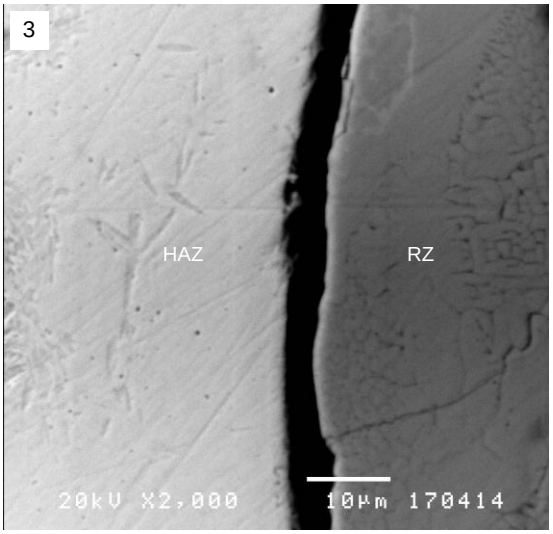

(b) Enlargement of the frame no.3

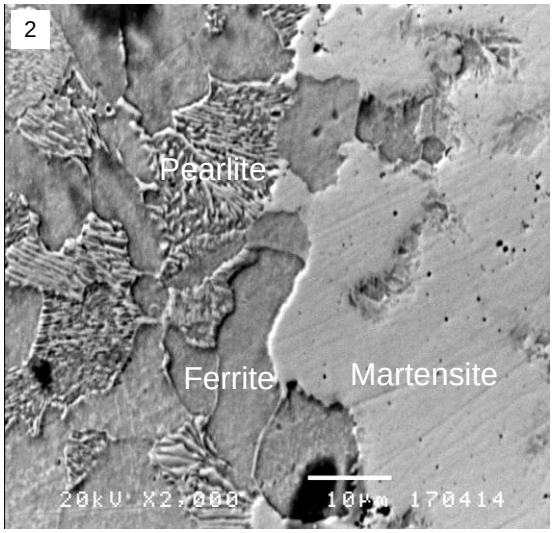

(c) Magnification 2,000x

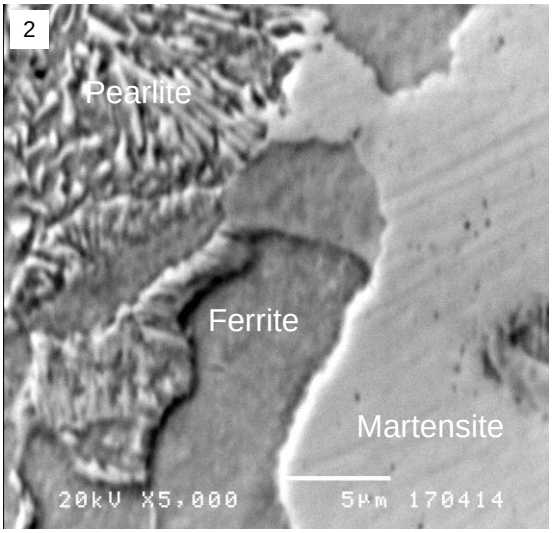

(d) Magnification 5,000x

Figure 4.14 SEM of HAZ boundary of the 1045 specimen

An EDS test was performed on the same the 1045 specimen to examine the distribution of C and Fe within the specimen. The test reveals the chemical composition had not changed for both the base area and HAZ area. Figure 4.15 (a) and (b) are the results of EDS test of the frame no.2 and no.3 as following mapping point of frame number in Figure 4.14 (a).

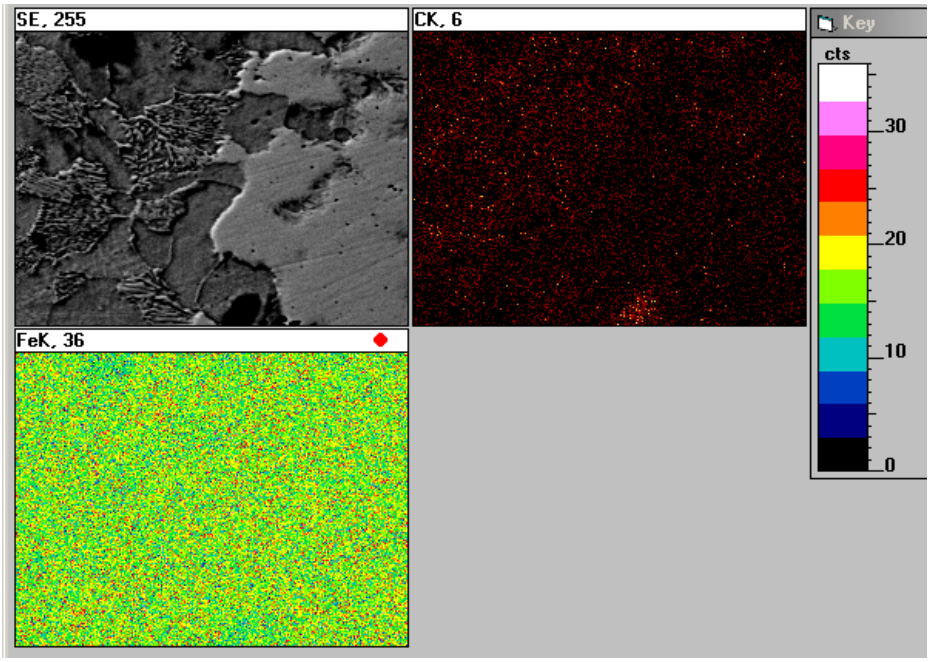

(a) EDS of the frame no.2

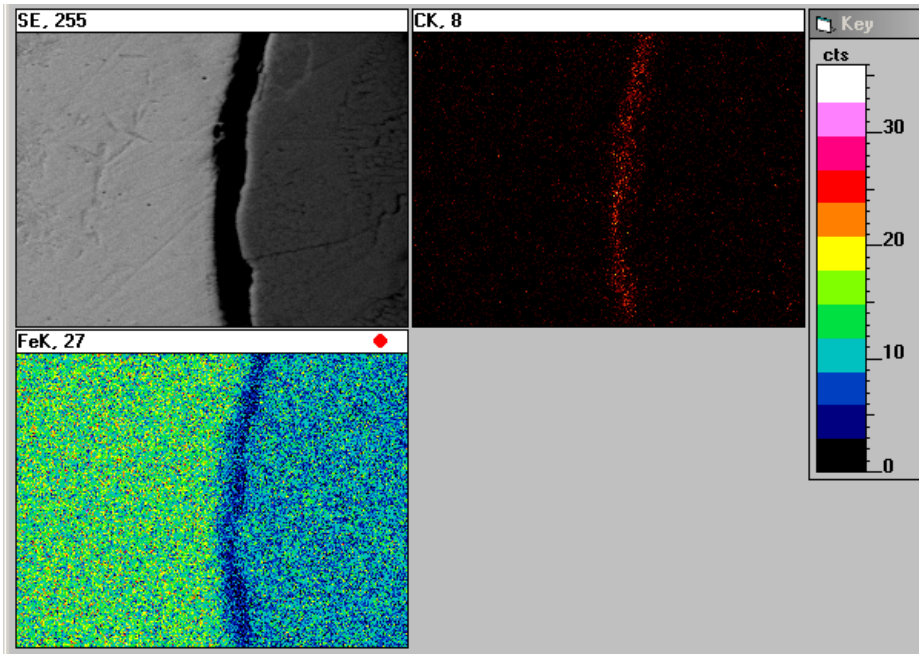

(b) EDS of the frame no.3

Figure 4.15 EDS of HAZ boundary of the 1045 specimen

4.3.4 Microhardness

A mechanical hardness test was performed on the 1045 specimen subjected to a laser power density of 60,000 W/cm^2, travelling speed 2 mm/s and distance 0.2 mm. Table 4.6 lists the results of from Micro-Vickers hardness tester, which refers to test point location shown in Figure 4.16. Table 4.6 shows dimensions of the indentation and hardness in units of HRC and HV. At a half of depth of HAZ, the hardness value about 700HV.

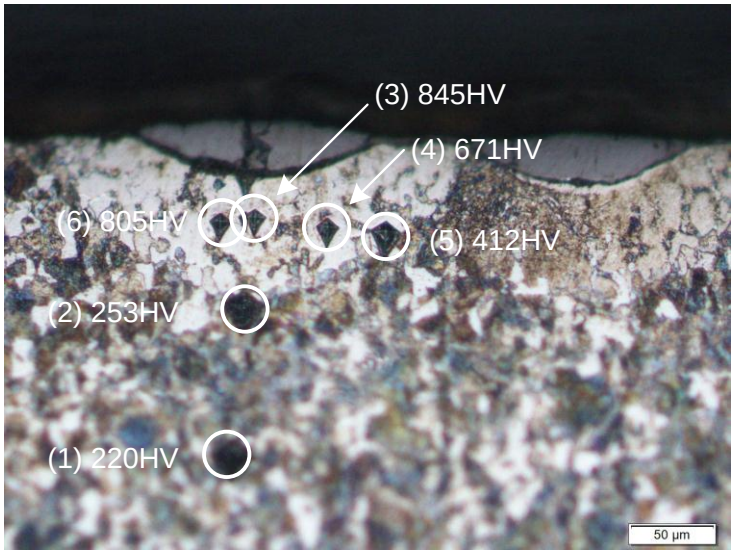

Figure 4.16 Measuring point of the 1045 specimen

Table 4.6 Hardness of the 1045 specimen by load 100 g, dwell 10 s

Point No.	D1(µm)	D2(µm)	HRC	HV
(1)	27.83	30.16	0.0	220.5
(2)	26.73	27.38	22.8	253.3
(3)	16.97	12.64	65.5	845.8
(4)	14.69	18.53	58.9	671.9
(5)	18.03	24.40	42.0	412.1
(6)	13.92	16.42	64.2	805.7

4.3.5 Opinions

1. The laser hardening process for the 1045 specimen was successful, except for the surface removal anomaly same also in case of the 4140 specimen. The Micro-Vickers hardness test for a sample without significant surface removal achieved at half the HAV depth, a hardness value of 800HV.

2. The flat black color spray point improved absorbability, but became unstable and behaved unpredictably, especially in instances there the laser beam overlapped as same as 4140 specimen.

CHAPTER 5 CONCLUSIONS AND SUGGESTIONS

1. The laser hardening process using a lower cost CO_2 laser was effective on metals with sufficient carbon content. The store bought, flat black spray paint was effective as an absorber, although it performed erratically, and unpredictably, and is suspected to have exacerbated surface removal on some of the samples. A more reliable absorbent coating; or perhaps a means to detect excessive surface temperature and adjust the laser power density accordingly would make this scheme more viable.

2. Seeing as this laser is not purpose built for laser hardening, accurate calibration is essential. The for optimum performance, the following specifications are suggested:
   - The laser beam should be applied at the focus point. The power density would be inadequate and difficult to gauge at any other point, especially a point outside of the outside of the depth of field range.
   - For this particular experiment, the diameter of the laser beam is 0.237 mm, the applied depth of field is 5.686 mm, the minimum resolution of the step setting for the CNC is 0.1 mm, and the minimum travelling speed setting is 1 mm/s.
   - The laser power percentage set at the control panel should be used in a range from 15 % to 90 %. The calculated values for laser power density based on current and voltage measurements were not linear, and thus corrected by way of linear regression. The set points for percent laser power shall correspond to the corrected values for power density.

3. Conclusion of results:
   - The SPHC steel sample could not be hardened by the laser because of insufficient carbon content.
   - The optimum parameters for laser surface hardening for the 4140 steel sample with minimum surface removal were found to be a: A laser power density of 70,000 W/cm^2, travelling speed of 8 mm/s, and a center-to-center distance for the individual lines was 0.2 mm. The mechanical hardness test yielded results of 704 HV at a depth of 90 microns, relatively half the depth of the HAV; resulting in a hardness increased from 323 HV to 704 HV.
   - The optimum parameters for laser surface hardening to the 1045 steel sample with minimum surface removal were found to be: A laser power density of 80,000 W/cm^2, a travelling speed of 8 mm/s and a center-to-center distance for the individual lines was 0.2 mm. The mechanical hardness tested yielded results of 845 HV at a depth of 83 microns, relatively half the depth of the HAV; resulting in a hardness increased from 220 HV to 845 HV.

4. Suggestions: further experimentation is warranted to determine if the results are repeatable for the respective sets of optimum parameters. A limiting factor was the open loop feedback control of this system. It would be helpful to provide a positive feedback loop that monitored laser power density and adjusted the control accordingly. Measuring the precise surface temperature of a very small area during the laser hardening process is difficult. If this can be achieved, it can be used as a means of an adaptive control to change the power density or a relevant process parameter.

REFERENCES

1. Grum, J., 2009, **Handbook of Thermal Process Modeling of Steels**, CRC Press, New York, USA, pp. 499-626

2. Kek, T. and Grum, J., 2010, **"Influence of the Graphite Absorber During Laser Surface Hardening"**, **Journal of Mechanical Engineering**, Vol. 56, pp. 150-157

3. Hecht, J., 2010, **"Short History of Laser Development"**, **Optical Engineering**, Vol. 49, pp. 1-23

4. Dahotre, N.B. and Harimkar, S.S., 2007, **Laser Fabrication and Machining of Materials**, Springer, New York, USA, pp. 23-66

5. Totten, G.E., 2006, **Steel Heat Treatment Handbook: Metallurgy and Technology**, CRC Press, New York, USA, pp. 8-44, 91-163

6. Dossett, J. and Totten, G.E., 2013, **ASM Handbook: Steel Heat Treating Fundamentals and Processes,** Vol. 4A, ASTM International, Materials Park, USA, pp. 476-502

7. Totten, G.E., Funatani, F., Xie, L. and Grum, J., 2004, **Handbook of Metallurgical Process Design,** CRC Press, New York, USA, pp. 641-732

8. Duarte, F.J., 1995, **Tunable Lasers Handbook,** Academic Press, California, USA, pp. 63-99

9. Selvan, J.S., Subramanian, K. and Nath, A.K., 1999, **"Effect of laser surface hardening on En18 (AISI 5135) steel", Journal of Materials Processing Technology**, Vol. 91, pp. 29–36

10. Lima, M.S.F, Goia, F.A., Riva, R. and Santo, A.M.E., 2007, **"Laser Surface Remelting and Hardening of an Automotive Shaft Sing a High-power Fiber Laser", Materials Research**, Vol. 10, No. 4, pp. 461-467

11. Fan, Y., Yang, Z., Cheng, P., Egland, K. and Yao, L., 2007, **"Investigation of Effect of Phase Transformations on Mechanical Behavior of AISI 1010 Steel in Laser Forming", Journal of Manufacturing Science and Engineering**, Vol. 129, pp. 110-116

12. Hussain, A., Ahmad, I., Hamdani, A.H., Nussair, A. and Shahdin, S., 2007, **"Laser surface alloying of Ni-plated steel with CO_2 laser", Applied Surface Science**, Vol. 253, pp. 4947–4950

13. Lakhkar, R.S., Shin, Y.C. and Krane, M.J.M., 2008, **"Predictive modeling of multi-track laser hardening of AISI 4140 steel", Materials Science and Engineering**, Vol.480, pp.209–217

14. Bailey, N.S., Tan, W. and Shin, Y.C., 2009, **"Predictive modeling and experimental results for residual stresses in laser hardening of AISI 4140 steel by a high power diode laser", Surface & Coatings Technology**, Vol. 203, pp. 2003-2012

15. Goia, F.A. and Lima, D., 2011, **"Surface Hardening of an AISI D6 Cold Work Steel Using a Fiber Laser", Journal of ASTM International**, Vol. 8, No. 2, Paper IDJAI103210.

16. Lütjering, G. and Williams, J.C., 2007, **Titanium,** 2nd ed., Springer, New York, USA, pp. 175-202

17. Henry, L., 2003, **Pipeline Engineering,** CRC Press, New York, USA, pp. 65-73

18. Chandler, H., 1995, **Heat Treater's Guide: Practices and Procedures for Irons and Steels**, 2nd ed., ASM International, Materials Park, USA, pp. 184-190, 319-325

APPENDIX A

Timeline of laser technology development

Table A.1 Timeline of laser technology development [3]

Year	Event
1916	- Albert Einstein proposes stimulated emission
1928	- Indirect evidence for stimulated emission reported by Rudolf Ladenburg
1940	- Light amplification by stimulated emission proposed by Valentin Fabrikant
1951	- Stimulated emission at 50 kHz observed by Edward Purcell and Robert Pound, Harvard
1954	- Charles Townes and James Gordon produce first microwave maser at 24 GHz at Columbia University
1957	- Townes starts investigating optical maser - Townes talks with Gordon Gould about optical pumping and optical maser - Gould coins the word laser and proposes Fabry-Pe´rot resonator in first notebook
1958	- Townes and Arthur Schawlow publish detailed optical maser proposal in Physical Review
1959	- Advanced Research Projects Agency issues $999,000 contract to TRG Inc. to develop laser based on Gould proposal
1960	- Theodore Maiman demonstrates ruby laser at Hughes Research Labs - TRG Inc. and Bell Labs duplicate ruby laser - Headlines announce laser discovery, predict uses from communications to weapons - Peter Sorokin and Mirek Stevenson, IBM, make first four-level solid-state laser, uranium in CaF_2 - Ali Javan, William Bennett, and Donald Herriott of Bell Labs make helium-neon laser, the first continuous-wave laser and the first gas laser
1961	- First neodymium laser in calcium tungstate, Leo Johnson and Kurt Nassau, Bell Labs - First neodymium-glass laser, Elias Snitzer, American Optical - Second harmonic of ruby generated by Peter Franken - Trion Instruments founded in Ann Arbor, MI, to make lasers - Quantatron founded by Maiman to make lasers; later becomes Korad - Ruby laser repairs detached retina in first patient at Harkness Eye Institute in New York
1962	- Red helium-neon laser invented by Alan White and Dane Rigden, Bell Labs - First semiconductor diode laser, Robert Hall, GE Research and Development Labs, followed in weeks by three other groups - Spectra-Physics and Perkin-Elmer introduce $8000 infrared helium-neon laser in March; sales take off when they introduce red version in autumn - Lawrence Livermore National Laboratory forms groups to study prospects for laser fusion - Air Force Chief of Staff Gen. Curtis LeMay praises prospects for laser nuclear defense
	(Continued)

Table A.1 Timeline of laser technology development (Continued)

Year	Event
1963	- Herbert Kroemer proposes heterostructures to improve diode lasers. Zhores Aleferov and Rudolf Kazarinov at Ioffe Institute in Russia file patent on double-heterostructure laser - First ion laser demonstrated in mercury by Earl Bell at Spectra-Physics - Nitrogen laser invented by H.G. Heard
1964	- Snitzer demonstrates first fiber amplifier - William Bridges discovers pulsed argon-ion laser at Hughes; Eugene Gordon develops continuous-wave argon at Bell - First three-dimensional laser holograms displayed by Emmett Leith and Juris Upatnieks - Kumar Patel makes CO_2 laser at Bell Labs - Joseph Geusic and LeGrand Van Uitert make first Nd:YAG laser at Bell
1965	- Kumar Patel reaches 200 W continuous wave from CO_2 laser - Coherent Radiation founded to manufacture CO_2 lasers - William Silfvast and Grant Fowles make helium-cadmium laser - J.V.V. Kasper and George C. Pimentel make first chemical laser, HCl - Coherent anti-Stokes Raman spectroscopy demonstrated by Robert Terhune at Ford
1966	- Peter Sorokin makes first dye laser at IBM; Fritz P. Schaefer independently invents dye at Max Planck Institute - Charles Kao and George Hockham propose communications through low-loss, single-mode optical fibers - Ed Gerry and Arthur Kantrowitz invent gas-dynamic CO_2 laser, which eventually reaches hundreds of kilowatts
1967	- Dye laser tuned for the first time by Bernard Soffer and B.B. McFarland at Korad - Jack Dyment develops stripe-geometry diode laser
1968	- Argon-laser treatment of diabetic retinopathy developed by Francis L'Esperance, Eugene Gordon, and Ed Labuda
1969	- Ruby laser pulses range the moon by bouncing off retroreflector placed by Apollo 11 astronauts
1970	- Nikolai Basov of Lebedev Institute reports pulsed ultraviolet lasing by xenon excimers - Zhores Alferov demonstrates first room-temperature continuous-wave diode laser - First low-loss optical fiber made by Robert Maurer, Donald Keck, and Peter Schultz at Corning - Ben Snavely demonstrates continuous-wave dye laser at Kodak
1971	- Rudolf Kazarinov and R.A. Suris propose concept behind quantum cascade laser
1972	- Erich Ippen and Charles Shank produce 1.5 ps pulses
1974	- First laser scanner demonstrated in a supermarket - Rare-gas halide excimer lasers invented; several types demonstrated - Two-photon Doppler-free spectroscopy developed independently by Theodor Ha¨nsch at Stanford and David Pritchard at MIT
	(Continued)

Table A.1 Timeline of laser technology development (Continued)

Year	Event
1976	- Bell Labs' accelerated aging tests predict million-hour lifetimes for GaAs diode lasers - J. Jim Hsieh operates InGaAsP diode emitting at 1.25mm at room temperature
1977	- John M.J. Madey operates first free-electron laser oscillator
1978	- MCA-Philips begins test marketing helium-neon laser player of 12 in. videodisks
1979	- Philips shows prototype compact disk player
1980	- Bell announces plans for TAT-8, first transatlantic fiber-optic cable - Supermarket scanners become common
1982	- Peter Moulton develops titanium-sapphire laser - Audio compact disk players introduced in Japan
1983	- Ronald Reagan launches Strategic Defense Initiative
1984	- First commercial diode-pumped neodymium lasers emit 100 mW continuous wave
1985	- Spectra Diode Labs introduces 200 mW array of ten continuous-wave GaAlAs diode laser stripes - Sony makes continuous-wave AlGaInP diode emitting at 671 nm in red - First room-temperature vertical cavity surface-emitting laser by Kenichi Iga
1986	- David Payne makes erbium-fiber laser tunable across 25 nm near 1535 nm
1987	- Payne reports 26 dB gain at 1536 nm in erbium-doped fiber amplifier - Pulses from dye laser compressed to 6 fs by Richard Fork at Bell
1988	- TAT-8, the first transatlantic fiber cable, is completed
1989	- Spectra Diode Labs produces 76 W continuous wave from 1 cm diode array - Isamu Akasaki demonstrates blue light-emitting diode of GaN
1994	- Nichia Chemical offers 450 nm nitride light-emitting diodes with 2% electrical conversion efficiency - Federico Capasso at Bell Labs demonstrates quantum cascade laser
1995	- Pulse length of titanium-sapphire reaches 8 fs
1996	- Shuji Nakamura of Nichia reports first blue diode laser, made from InGaN
2000	- Titanium-sapphire pulses compressed to 5 fs - Peak of technology stock bubble; the American stock exchange NASDAQ exceeds 5000 during the 2000 Optical Fiber Communication Conference and Exposition.
2002	- TAT-8 submarine cable retired after failure because its capacity was too small to justify the cost of repairs
2004	- Ozdal Boyraz and Bahrom Jalali, first silicon Raman laser at the University of California, Los Angeles
2006	- John Bowers, first silicon laser
2007	- John Bowers and Brian Koch, first mode-locked silicon evanescent laser
2010	- First 10 petawatt laser at Lawrence Livermore National Laboratory

APPENDIX B

Electromagnetic spectrum

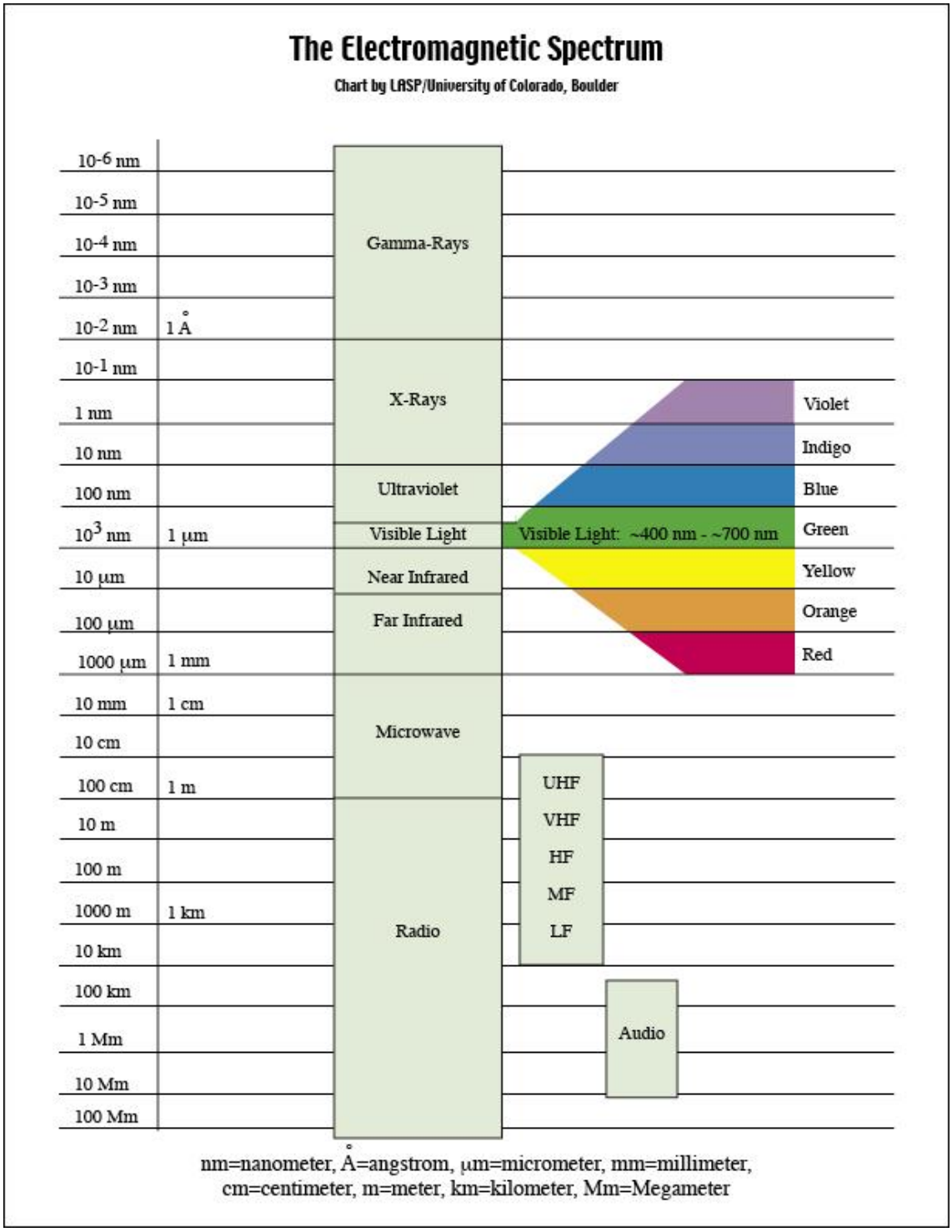

Figure B.1 The electromagnetic spectrum [4]

APPENDIX C

Types of industrial lasers

Table C.1 Types of industrial lasers

Category of lasers	**Type of Lasers**	**Wavelength, (nm)**
Solid-state lasers	Nd:YAG	1064
	Ruby	694
	Nd:glass	1062
	Alexandrite	700-820
	Titanium-sapphire	700-1100
	Er:YAG	2940
	Nd:YLF	1047
Gas laser	HeNe	632.8
	Argon	488, 514.5
	Krypton	520-676
	HeCd	441.5, 325
	CO_2	10600
	CO	2600-4000, 4800-8300
	ArF	191
	KrF	249
	XeCl	308
	XeF	251
	Copper vapor	510.6, 578.2
	Gold vapor	628
Semiconductor lasers	InGaAs	980
	AlGaInP	630-680
	InGaAsP	1150-1650
	AlGaAs	780-880
Liquid dye lasers	Rhodamine 6G	570-640
	Coumarin 102	460-515
	Stibene	403-428

APPENDIX D

Iron-Carbon Equilibrium Diagram

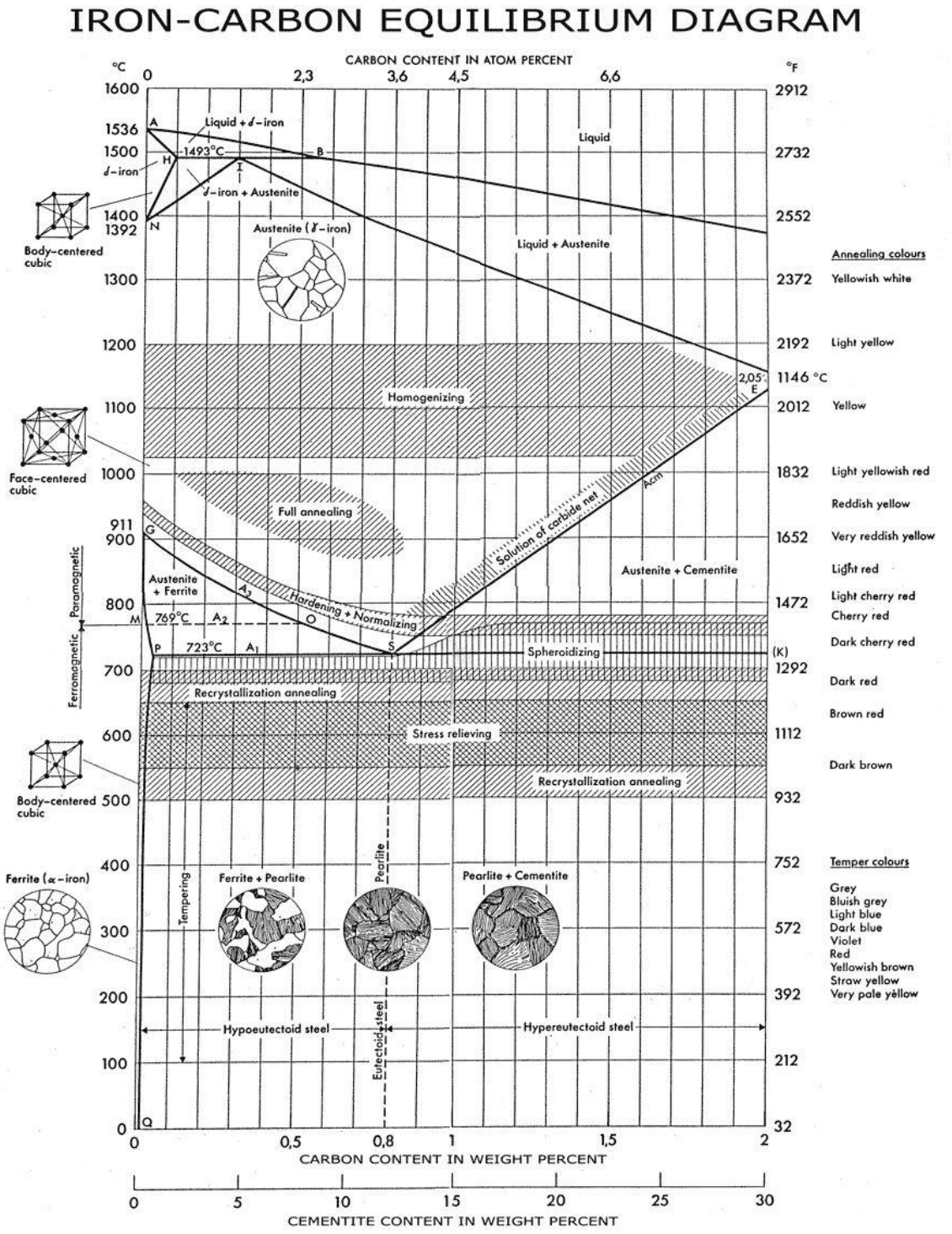

Figure D.1 Iron-Carbon Equilibrium Diagram

APPENDIX E

Laser System Specifications

CO_2 Laser Tube:

Model/Manufacturer	: TLC700-50/OEM
Wavelength (λ)	: 10.6 µm
Spot diameter (d_B)	: 3.5 mm.
Maximum output power	: 40 W
Triggering voltage	: 18-20 KV
Operating voltage	: 14-15 KV
Operating current	: 0-22 mA
Outer diameter	: 50 mm.
Length	: 700 mm.
Power stability	: <10%
Light Beam Quality (M)	: <1.2
Life hours	: 1,000-1,300 Hours

CNC:

Model/Manufacturer	: NA/OEM
Speed	: 1–35 mm/s
Working Area	: 300x200 mm.
Resolution Ratio	: 0.1 mm.

CNC Controller:

Model/Manufacturer	: HT-XEON/Lihuiyu Studio Labs
S/N	: NA

Reflective mirror:

Model/Manufacturer	: NA/OEM
Material	: K9 optical glass (borosilicate glass)
Diameter	: 20 mm.
Thickness	: 3 mm.
Coating	: Gold-coating

Focusing lens:

Model/Manufacturer	: NA/OEM
Material	: ZnSe (Zinc-Selenide)
Diameter	: 12 mm.
Focal distance (F)	: 50.8 mm.
Edge thickness	: 2 mm.
Focus beam diameter	: 0.2 mm.

Software:

Model/Manufacturer	: LaserDRW/Lihuiyu Studio Labs
Operation System	: Windows 7

APPENDIX F

Temper colors chart

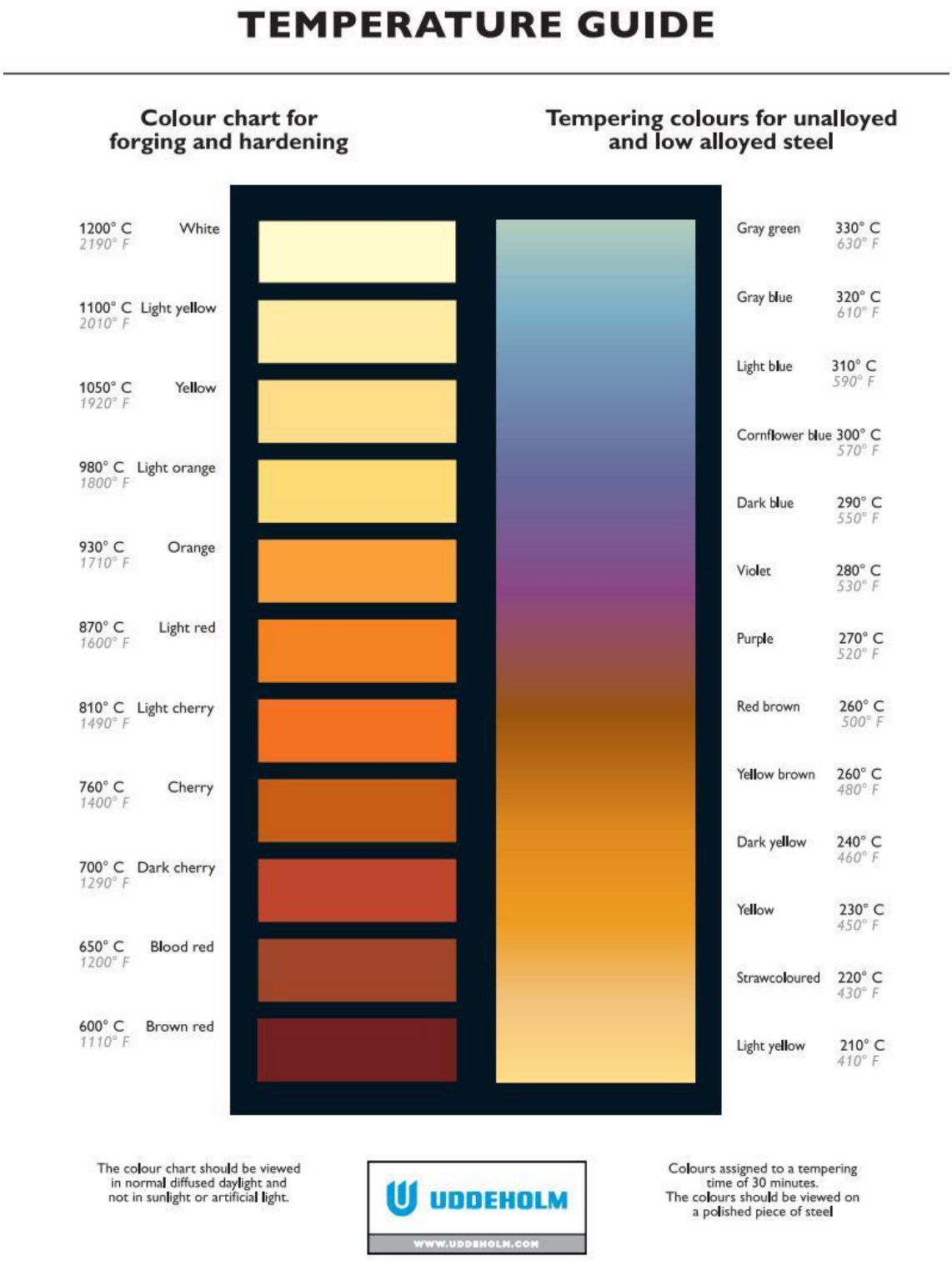

Figure F.1 Temper colors chart

CURRICULUM VITAE

Name Mr.Bhavin Bhatrasupong

Date of Birth November 22th, 1970

Educational Record

Bachelor's Degree — Bachelor of Industrial Technology (Electronics)
King Mongkut's Institute of Technology North Bangkok

Master's Degree — Master of Engineering (Metallurgical Engineering)
King Mongkut's University of Technology Thonburi

Employment Record

Mechanical & Electrical Specialist
Energy Resourcing Group (Thailand) Ltd., 2012 – 2013

QA/QC Welding Inspector
PTT Global Chemical Plc., 2011 – 2012
PTT Aromatics and Refining Plc., 2010 – 2011

Project Manager // QMR
Prompt Technical Services Limited, 2007 – 2009

Senior Engineer
Chemitreat (Thailand) Co.,Ltd., 2005 – 2007

Engineering Support Division Chief
Advanced Technology Contracting Co.,Ltd., 2002 – 2005

Application Engineer
Complex Technology Co., Ltd., 1992–2002

มหาวิทยาลัยเทคโนโลยีพระจอมเกล้าธนบุรี

ข้อตกลงว่าด้วยการโอนสิทธิในทรัพย์สินทางปัญญาของนักศึกษาระดับบัณฑิตศึกษา

วันที่.....28.....เดือน....พฤษภาคม..... พ.ศ..2557.....

ข้าพเจ้า (นาย/~~นาง/นางสาว~~).....ภวินญ์ ภัทรสุพงศ์.....รหัสประจำตัว....55070701209....
เป็นนักศึกษาของมหาวิทยาลัยเทคโนโลยีพระจอมเกล้าธนบุรี
ระดับ ○ ประกาศนียบัตรบัณฑิต ☑ ปริญญาโท ○ ปริญญาเอก
หลักสูตร...วิศวกรรมมหาบัณฑิต..... สาขาวิชา..วิศรกรรมโลหการ.....คณะ.....วิศวกรรมศาสตร์.....
อยู่บ้านเลขที่..143/101..หมู่..-...ตรอก/ซอย..-...ถนน..ริมคลองประปา.....ตำบล/แขวง..บางซื่อ.....
อำเภอ/เขต.....บางซื่อ.....จังหวัด.....กรุงเทพฯ.....รหัสไปรษณีย์.....10800.....
เป็น "ผู้โอน"ขอโอนสิทธิในทรัพย์สินทางปัญญาให้ไว้กับมหาวิทยาลัยเทคโนโลยีพระจอมเกล้าธนบุรี โดยมี **รศ.ดร.สักกมน เทพหัสดิน ณ อยุธยา** ตำแหน่ง **รองคณบดีฝ่ายวิจัยและวิชาการ** คณะวิศวกรรมศาสตร์ เป็นตัวแทน "ผู้รับโอน" สิทธิในทรัพย์สินทางปัญญาและมีข้อตกลงดังนี้

1. ข้าพเจ้าได้จัดทำโครงงานวิจัยอุตสาหกรรมเรื่อง การเพิ่มความแข็งผิวโลหะด้วยคาร์บอนไดออกไซด์เลเซอร์และการเคลือบผิวด้วยสีดำ (Surface hardening of steels by using a CO_2 laser with black color coating) ซึ่งอยู่ในความควบคุมของ ดร.ไพบูลย์ ช่วงทอง อาจารย์ที่ปรึกษา และ ดร.วิบุญ ตั้งวโรดมนุกูล อาจารย์ที่ปรึกษาร่วม ตามพระราชบัญญัติลิขสิทธิ์ พ.ศ. 2537 และถือว่าเป็นส่วนหนึ่งของการศึกษาตามหลักสูตรของมหาวิทยาลัยเทคโนโลยีพระจอมเกล้าธนบุรี

2. ข้าพเจ้าตกลงโอนลิขสิทธิ์จากผลงานทั้งหมดที่เกิดขึ้นจากการสร้างสรรค์ของข้าพเจ้าในโครงงานวิจัยอุตสาหกรรมให้กับมหาวิทยาลัยเทคโนโลยีพระจอมเกล้าธนบุรี ตลอดอายุแห่งการคุ้มครองลิขสิทธิ์ตามพระราชบัญญัติลิขสิทธิ์ พ.ศ. 2537 ตั้งแต่วันที่ได้รับอนุมัติโครงร่างโครงงานวิจัยอุตสาหกรรมจากมหาวิทยาลัย

3. ในกรณีที่ข้าพเจ้าประสงค์จะนำโครงงานวิจัยอุตสาหกรรมไปใช้ในการเผยแพร่ในสื่อใดๆ ก็ตาม ข้าพเจ้าจะต้องระบุว่าโครงงานวิจัยอุตสาหกรรมเป็นผลงานของมหาวิทยาลัยเทคโนโลยีพระจอมเกล้าธนบุรีทุกครั้งที่มีการเผยแพร่

4. ในกรณีที่ข้าพเจ้าประสงค์จะนำโครงงานวิจัยอุตสาหกรรมไปเผยแพร่ หรือให้ผู้อื่นทำซ้ำหรือดัดแปลงหรือเผยแพร่ต่อสาธารณชนหรือกระทำการอื่นใด ตามพระราชบัญญัติลิขสิทธิ์ พ.ศ. 2537 โดยมีค่าตอบแทนในเชิงธุรกิจ ข้าพเจ้าจะกระทำได้เมื่อได้รับความยินยอมเป็นลายลักษณ์อักษรจากมหาวิทยาลัยเทคโนโลยีพระจอมเกล้าธนบุรีก่อน

5. ในกรณีที่ข้าพเจ้าประสงค์จะนำข้อมูลจากโครงงานวิจัยอุตสาหกรรมไปประดิษฐ์หรือพัฒนาต่อยอดเป็นสิ่งประดิษฐ์หรืองานทรัพย์สินทางปัญญาประเภทอื่น ภายในระยะเวลาสิบ (10) ปีนับจากวันลงนามในข้อตกลงฉบับนี้ ข้าพเจ้าจะกระทำได้เมื่อได้รับความยินยอมเป็นลายลักษณ์อักษรจากมหาวิทยาลัยเทคโนโลยีพระจอมเกล้าธนบุรี และมหาวิทยาลัยเทคโนโลยีพระจอมเกล้าธนบุรีมีสิทธิในทรัพย์สินทางปัญญานั้น พร้อมกับได้รับชำระค่าตอบแทนการอนุญาตให้ใช้สิทธิดังกล่าว รวมถึงการจัดสรรผลประโยชน์อันพึงเกิดขึ้นจากส่วนใดส่วนหนึ่งหรือทั้งหมดของโครงงานวิจัยอุตสาหกรรมในอนาคต โดยให้เป็นไปตามระเบียบสถาบันเทคโนโลยีพระจอมเกล้าธนบุรี ว่าด้วย การบริหารผลประโยชน์อันเกิดจากทรัพย์สินทางปัญญา พ.ศ. 2538

6. ในกรณีที่มีผลประโยชน์เกิดขึ้นจากโครงงานวิจัยอุตสาหกรรมหรืองานทรัพย์สินทางปัญญาอื่นที่ข้าพเจ้าทำขึ้นโดยมีมหาวิทยาลัยเทคโนโลยีพระจอมเกล้าธนบุรีเป็นเจ้าของ ข้าพเจ้าจะมีสิทธิได้รับการจัดสรรผลประโยชน์อันเกิดจากทรัพย์สินทางปัญญาดังกล่าวตามอัตราที่กำหนดไว้ในระเบียบสถาบันเทคโนโลยีพระจอมเกล้าธนบุรี ว่าด้วย การบริหารผลประโยชน์อันเกิดจากทรัพย์สินทางปัญญา พ.ศ. 2538

ลงชื่อ.....ผู้โอนลิขสิทธิ์

(นายภวินญ์ ภัทรสุพงศ์)

นักศึกษา

ลงชื่อ.....ผู้รับโอนลิขสิทธิ์

(รศ.ดร.สักกมน เทพหัสดิน ณ อยุธยา)

รองคณบดีฝ่ายวิจัยและวิชาการ

ปฏิบัติการแทนคณบดี

ลงชื่อ.....พยาน

(ดร.ไพบูลย์ ช่วงทอง)

ลงชื่อ.....พยาน

(ผศ.ดร.ไชยา ดำคำ)